University of Alberta
Department of Civil Engineering

Structural Engineering Report No. 20

Composite Beams in Negative Bending

by
J.H. Davison
and
J. Longworth

May, 1969

COMPOSITE BEAMS IN NEGATIVE BENDING

by

J. H. DAVISON

J. LONGWORTH

May, 1969

Department of Civil Engineering
University of Alberta
Edmonton, Canada

ABSTRACT

The objective of this investigation was to determine the effect of longitudinal slab reinforcement on the moment and rotation capacities of composite beams in an isolated negative moment region. Eight tests were performed on beams with varying slab widths and amounts of reinforcement. A relatively stocky WF section was employed to minimize the possibility of premature failure due to local buckling. All beams exhibited large rotations after yielding occurred at the location of the negative plastic hinge. Failure was initiated by local buckling in the web. Unloading was gradual after the subsequent development of a local buckle in the compression flange.

It was concluded that significant increases in the negative moment capacity of composite beams can be achieved by the addition of longitudinal slab reinforcement, but that these increases are not in proportion to theoretical simple plastic moment values. The exact contribution of the longitudinal steel cannot be established from the present investigation but is related to the effect of the reinforcement on the stability conditions of the web. As the amount of longitudinal slab reinforcement is increased, the rotation capacity of the negative plastic hinge decreases. It was also concluded that, for any given amount of longitudinal reinforcement, variation in slab width up to a maximum of 6'-0" has no significant effect on ultimate moment capacity or rotation capacity of the composite section.

TABLE OF CONTENTS

CHAPTER I

INTRODUCTION

1.1 INTRODUCTORY REMARKS

The present investigation forms a part of a continuing study of continuous composite beams being carried out in the Department of Civil Engineering at the University of Alberta. The object of the study is to describe the behavior of continuous composite beams over the full range of loading to failure and to propose design criteria based on ultimate load.

Composite construction has long been recognized as an economical means of resisting positive moment. However, behavior in negative moment is not as well understood, particularly with respect to the contribution of longitudinal slab reinforcement. As a result, common design practice ignores any contribution of longitudinal slab reinforcement to the negative moment capacity even though significant amounts of such steel are used to control cracking. Thus the advantage of a greatly increased positive moment capacity in a continuous beam is somewhat offset by considering only the contribution of the steel section in resisting negative moment. In addition, if longitudinal slab reinforcement could be reliably counted upon to resist negative moment, a substantial advantage would result in tall buildings due to the increased lateral stiffness of the structure. Thus it is the purpose of this investigation to study the behavior of composite beams

subjected to negative moment.

1.2 REVIEW OF PREVIOUS RESEARCH

The behavior of composite beams under positive moment has been thoroughly investigated. However, knowledge of the behavior of composite beams under negative moment is limited. As far as can be ascertained the preceding investigation in the present study, by Piepgrass[1] in 1968, represented the first attempt to isolate the negative moment region. Several investigations of continuous members have been undertaken and a brief summary of their main conclusions follows.

In 1953 Siess and Viest[2] tested two quarter scale composite bridge decks, one with shear connectors throughout, and the other with shear connectors only in the positive moment region. It was concluded that the slab reinforcing in the negative moment region was fully effective in contributing to the moment capacity of the section in the case where shear connectors were provided throughout.

In 1961 Culver, Zarzeczny and Driscoll[3] tested a continuous composite beam to establish the feasibility of designing such a beam by plastic methods. The concrete slab was not reinforced in the transverse direction and failure in the negative moment region resulted from the formation of a large longitudinal crack along the centreline of the beam. Temperature steel in the longitudinal direction was not taken into account in computing the plastic moment capacities of the section. It was concluded that only the steel beam could be considered as effective over the negative moment region,

and that an expansion joint should be provided in negative moment regions in the slab to sustain the large rotations.

In 1962 Slutter and Driscoll[4] tested one continuous composite member to investigate the applicability of plastic analysis along with ultimate strength design. It was concluded that the longitudinal slab reinforcement could be included when computing the plastic moment capacity of the composite section in the negative moment region, provided shear connectors were present, but that redistribution of moments could be permitted only in the case where negative hinges were first to form, due to the limited rotation capacity of the positive moment section.

In 1963 Barnard [5] tested a series of four continuous three-span composite beams, two of which failed by crushing of the concrete in the positive moment regions, while the other two failed due to an S-shape buckle of the steel section in the negative moment region. On the basis of these tests Barnard concluded that slab reinforcing could confidently be used to strengthen the negative moment regions, provided buckling and shear failure could be avoided.

In 1966 Daniels and Fisher[6,7] tested four two-span continuous composite steel-concrete beams first under fatigue loading and, subsequently, statically to ultimate load. It was concluded that sufficient shear capacity remained after the fatigue tests to develop the flexural strength of the beam. It was also concluded that simple plastic analysis and ultimate strength theory, including the contribution of the tensile strength of the longitudinal reinforcement in the slab, could be used for design of continuous composite

members. However Daniels and Fisher warned that local flange and web buckling near the interior support limits the ultimate load carrying capacity of the member and recommended further research to establish design rules which would allow the full negative plastic hinge to develop prior to flange and web local buckling.

1.3 PRIOR INVESTIGATIONS WITHIN THE PRESENT STUDY

The present investigation is the third in a continuing study of the behavior of composite beams. The initial investigation by Ferrier[8] in 1965 concerned itself primarily with the development of moment-curvature relationships for composite beams subjected to positive moment. A method of analysis based on simplifying assumptions was developed, and an empirical means suggested for predicting the curvature corresponding to the bending moment at failure. Tests were performed on four simply-supported beams, which represented two extremes in slab to steel beam proportioning. Test results were in good agreement with the analysis.

The second investigation within the study, by Piepgrass[1] in 1968, was concerned, as is the present investigation, with the behavior of composite beams in an isolated negative moment region. The two major variables were the amount of longitudinal slab reinforcement and the width of slab. A total of six beams were tested. Beams 1, 2, 3, and 4 contained longitudinal reinforcement in the amount of 3.10, 2.48, 1.86 and 1.20 square inches respectively. Each had a 3'-0" slab width. Together with Beam 2, Beams 5 and 6 were designed to show the effect of varying slab widths, from 3'-0" to 5'-0". All these beams contained 2.48 square inches of longitudinal

slab reinforcement. All slabs were 3 inches thick. The steel section used throughout was a 12B16.5, but because of the poor rotation capacities exhibited by Beams 3 and 4 due to premature local buckling of the steel section, the compression flanges of the remaining test specimens were stiffened with a 3" x 3/8" cover plate. Beam 4 was unloaded before destruction, cover plated and subsequently re-tested to failure as Beam 4A. The width-thickness ratios of the 12B16.5 were 46.7 for the web, and 7.43 for the compression flange. Canadian Standards Association, Standard S16-1965, Steel Structures For Buildings[9], classifies a 12B16.5 as a compact section for G40.12 steel, but the width-thickness ratios are near the maximum values permitted. The cover plated compression flange had an effective width-thickness ratio of 6.0.

The beams failed in a variety of modes. Failure of Beam 3 was initiated by the formation of local buckles in the web and compression flange. It was not possible to determine which buckle was the first to form. In the case of Beam 4, visual observation suggested that the failure started in the web. Beams 1, 4A, 5 and 6 all failed in a lateral buckling mode. Beam 2 failed due to separation of the cover plate from the compression flange which initiated local buckling.

The ratio of moment at failure to the computed plastic moment capacity of the section ranged from 0.98 to 1.07. All beams exhibited little rotation capacity. It was noted that the average stress in the longitudinal slab reinforcement at ultimate moment was less than the yield stress for the reinforcement. It was therefore

concluded that use of a steel beam section defined as compact under the provisions of CSA Standard S16 did not guarantee adequate rotation capacity for the formation of a plastic hinge in a composite beam in negative bending.

1.4 SCOPE OF THE PRESENT INVESTIGATION

The primary objective of the present investigation is to further study the effect of longitudinal slab reinforcement on the moment and rotation capacities of composite beams in an isolated negative moment region. A secondary objective is to further study the effect of varying slab widths on the behavior of such beams. On the basis of the work by Piepgrass, it is evident that reduction in rotation capacity due to premature local and lateral buckling must be avoided before the formation of a plastic hinge in the negative moment region if the above objectives are to be realized.

CHAPTER II

TEST PROGRAM

2.1 DESIGN OF TEST SPECIMENS

2.1.1 CHOICE OF A STEEL SECTION

From the previous investigation within this study, it was evident that the proportions of the steel section were critical in limiting the rotation capacity of the composite beam. In order to effectively investigate the influence of the longitudinal slab reinforcement, it was felt that buckling of the compression elements of the steel section had to be prevented until an effective negative plastic hinge could be formed. It was assumed that lateral buckling of the compression flange could be prevented by employing suitable lateral bracing. Thus the criterion for the selection of a suitable steel section became one of resistance to local buckling.

The physical behavior of a composite beam with longitudinal slab reinforcement when subjected to negative moment is similar to that of a beam-column. The tension force in the reinforcement acts as a longitudinal load on the steel section. This longitudinal load is transmitted to the steel section through the shear connectors. CSA Standard S16[9] limits the depth-thickness ratios of webs of compact sections when subjected to axial compression plus bending to $255/\sqrt{F_y}$. Similarly, to preclude the possibility of local buckling until the onset of strain-hardening, CSA Standard S16 limits the width-thickness ratio of the projecting elements of the compression

flange to $54/\sqrt{F_y}$. For CSA G40.12 steel these ratios are 40.3 and 8.54 respectively.

On this basis, and considering size limitations, a 12WF36 was selected as the steel section to be used throughout the test series. For this section the h/w and b/t ratios for the web and flange respectively are 34.0 and 6.07. In comparison, the corresponding ratios for a 12B16.5, as used by Piepgrass[1], are 46.7 and 7.43. Ferrier[8] employed a 12WF36 in his positive moment investigation, and therefore, later comparisons of negative and positive moment behavior may be made.

2.1.2 PROPORTIONING OF COMPOSITE SECTIONS

A slab thickness of 4 inches was selected, with the longitudinal reinforcement placed at its mid-depth. The span length was chosen as 8'-0", with the overall length of 10'-0" allowing for 1'-0" anchorage of reinforcement at each end. This length of negative moment region was considered compatible with a span length in the order of 20 feet, which might be considered in the practical range for a continuous span.

The greatest positive moment capacity of Ferrier's beams was approximately 2.2 times the plastic moment capacity of the steel section alone. Adding enough reinforcement to bring the neutral axis to the tension flange in the region of maximum negative moment corresponds to increasing the plastic negative moment capacity of the composite section to approximately 1.4 times that of the steel section. These two conditions represent the most severe case of moment gradient

likely to be encountered. In this condition a 4'-0" negative moment region corresponds to a 20' span using simple plastic analysis.

For positive moment CSA Standard S16 allows a maximum effective flange width of 5'-10" for a 4" slab, provided the span length is at least four times the effective flange width. A standard slab width of 4'-0" was selected. Such a width falls within the effective width limitations of CSA Standard S16 for a 20'-0" span.

2.1.3 LONGITUDINAL SLAB REINFORCEMENT

Increasing the amount of longitudinal slab reinforcement in a negative moment region moves the neutral axis towards the slab. When the neutral axis reaches the tension flange, additional reinforcement only slightly increases the plastic moment capacity of the section. For this reason, 3.68 square inches of reinforcing steel (12 #5 bars), enough to place the neutral axis of the fully plastic section in the tension flange, was selected as an upper bound for the longitudinal reinforcement. Beams 11 to 14 (see TABLE 2.1) were designed to indicate the effect of the amount of longitudinal reinforcement on the moment and rotational capacities of the section.

Three beam specimens were designed to indicate the effect of slab width on the behavior in negative bending. A maximum slab width of 6'-0" was selected as being slightly beyond the effective flange width permitted under CSA Standard S16. Beam 15 had the same ratio of area of reinforcement to area of concrete as Beam 13, and Beam 16 the same ratio as Beam 14. Beam 17 provided a steel area identical to Beams 13 and 16, in the maximum 6'-0" width. A length

of 12WF36 without a slab was tested as Beam 18 to provide a reference for comparison. FIGURE 2.1 shows a typical cross-section of the composite beams. Details of the test specimens are given in TABLE 2.1.

Sufficient shear connectors were provided to withstand the force in the longitudinal reinforcement at yield and were spaced uniformly throughout the span. The capacity of 3/4"ø x 3" headed stud shear connectors was taken as 11.5 kips, and that of 7/8"ø x 3½" headed stud shear connectors as 15.6 kips, the allowable horizontal shear loads permitted by CSA Standard S16 for concrete with a compressive strength of 3000 psi. Transverse slab reinforcement consisted of #3 bars spaced at 6 inches or 4½ inches. Thus the area of transverse steel was 2.29 or 3.02 times that normally provided for temperature and shrinkage requirements. Bearing stiffeners were provided at the load and reactions points. FIGURE 2.2 shows the details of the fabricated steel section.

2.2 DESIGN OF TESTING APPARATUS

2.2.1 DESIGN OF LATERAL BRACING

In the selection of a suitable steel section for the test series it was assumed that lateral buckling of the compression flange could be prevented by employing appropriate lateral bracing. CSA Standard S16 permits an unbraced length of 360 $r_y/\sqrt{F_y}$ between the location of a plastic hinge and a point of zero moment. To account for the possibility of the entire web being in compression, r_y was calculated as the effective radius of gyration of a section comprising the entire web and compression flange. For a 12WF36 the value of this effective radius of gyration is 1.33 inches. Thus, for G40.12 steel,

the maximum allowable unbraced length is 75 inches. Accordingly lateral bracing at midspan and at the reaction points should preclude the possibility of premature lateral buckling of the compression flange.

Tie rods were utilized to brace the beam at the reaction points. An articulated brace laterally supported the compression flange at midspan, but still allowed the beam to deflect. The lateral braces were attached to lugs welded to the compression flange at the reaction points and to a 1 $^{3}/_{16}$" diameter pin attached at midspan. These details are shown in FIGURE 2.2

2.2.2 TESTING EQUIPMENT

The specimens were tested with the slab on the underside. A roller support unit, fitted with a rocker-plate assembly, and seated on a concrete pedestal was provided at each reaction. The slab was set in plaster of Paris to ensure a uniform bearing.

The test beams were loaded by means of a single 220 kip Amsler jack at midspan. A "loading bridge" distributed the load from the jack as two line loads across the compression flange, each 5" from midspan. This bridge also permitted adequate rotation of the centre portion of the articulated brace to allow for the expected deflections. A load frame provided support for the jack and the lateral bracing. Schematic plan and elevation views of the testing apparatus are shown in FIGURE 2.3. Photographs of the test set up are shown in PLATE 2.1.

2.3 PRELIMINARY TEST

A preliminary test beam of the same proportions as Beam 13 was fabricated and tested with minimum instrumentation to determine the suitability of the test sections and to check the performance of the testing apparatus. The specimen exhibited good rotational capacity, failing by local buckling of the web and compression flange after large deflections were achieved. The test set-up proved satisfactory in providing adequate lateral support and permitting the required deflections. On the basis of this preliminary test no modifications were made to the test specimens or loading arrangement.

2.4 FABRICATION OF TEST SPECIMENS

All steel beam sections were fabricated from G40.12 material of the same heat lot. Fabrication included the installation of bearing stiffeners, shear connectors, and attachment lugs for the lateral bracing. A 10'-0" length of the 12WF36 section was provided for the determination of material properties. Electrical resistance strain gages were attached to the steel section before placement in the forms for the casting of the concrete slab.

The slab reinforcing bars were ground smooth at the strain gage locations and were then tied into mats. To allow for the placement of the gages, Styrofoam blocks, which could be chipped out after the concrete had hardened, were placed at all gage locations. PLATE 2.2 shows the fabricated steel specimen and the reinforcing mats in position prior to casting.

Concrete for the test beams was mixed in a 9 cubic foot Eirich mixer in the University of Alberta Structures Laboratory and

was controlled to approximately 3½" slump. A mechanical vibrator was used in the placement of the concrete in the forms. Six test cylinders were poured with each beam. The beams were moist cured for 3 days, and then allowed to cure under laboratory conditions for a period which ranged from 39 to 71 days before testing.

After the beam was positioned in the testing apparatus and the strain gages connected to the Dymec Data Acquisition System, the steel section was white-washed so that the progression of yielding throughout the specimen might be followed.

2.5 MATERIAL PROPERTIES

The mix proportions and results of the concrete cylinder tests are given in Appendix A. Also shown are the results of tensile tests on coupons cut from the web and flanges of the steel section, and on lengths of the different sizes of reinforcing bars used.

2.6 INSTRUMENTATION

SR4-A7 electrical resistance strain gages were used to measure strains in the slab reinforcement and the steel section. Locations of the gages on the reinforcing bars are shown in FIGURE 2.4. Single gages were positioned at mid-length of six transverse reinforcing bars. Each longitudinal bar was instrumented with a single gage at midspan. In addition, the two innermost and the two outermost longitudinal bars were provided with gages located 1'-6" on either side of midspan. A total of fourteen strain gages were located on the steel section, all at midspan, as shown in FIGURE 2.5.

Deflections were measured by displacement transducers. Two

7DCDT-1000 transducers (±1" travel) were installed on the tension flange of the steel section at midspan, one on each side of the web. Two 7 DCDT-3000 transducers (±3" travel) were used to measure the deflections of the slab extremities at midspan. All transducers were operated on a DC power supply at 6.0 volts.

The strain gages were connected through a balance box - power supply unit into a Dymec 2010J Data Acquisition System. The transducers were connected directly to the Data Acquisition System. The Dymec system consists basically of an integrating digital voltmeter and a channel scanner. Output from the voltmeter can be recorded on magnetic tape and/or a paper printout. The latter was used in this case. Thus all strain and deflection readings were automatically recorded after each load increment.

Mechanical dial gages, positioned on the slab on each side of the steel section, provided a visual indication of equilibrium under a given load.

2.7 TEST PROCEDURE

The Dymec Data Acquisition System was allowed to warm up at least an hour before each test. Immediately prior to loading the electrical resistance strain gage circuits were balanced to ensure an initial reading as close as possible to zero. At the beginning of each test a load of approximately 100 pounds was applied and initial strain and deflection readings recorded. At this time shrinkage cracks in the concrete were marked.

Load was increased in increments of 10 kips until the

additional deflection for a given load increment became much greater than that for the previous increment. At this point the load maintainer on the Amsler jack was released, and further loads were held manually. The size of further load increments was based mainly on deflection considerations. After each increment of load was applied and equilibrium achieved, strain and deflection readings were taken and additional cracking of the slab marked. The load maintainer was not used near failure so that if deflections did not stabilize, i.e. equilibrium could not be achieved under a given load, the load could be reduced to obtain points on the falling portion of the load-deflection curve.

Tests were continued to the full extension of the jack which resulted in deflections greater than 4 inches. At these deflections all beams were well into the unloading branch of the load-deflection curve and all had developed large web and flange local buckles.

During the testing of Beam 16, one side deflected at a faster rate than the other, producing an overall rotation of the specimen. The specimen was unloaded and shims placed under the load distribution bridge to maintain the load in a vertical position. No subsequent difficulty was encountered. A similar situation occurred in the test of Beam 18 (WF alone) due to twist buckling. The problem was satisfactorily handled in the manner described above.

Crack patterns in the slabs were outlined and photographed when the specimens were removed from the loading apparatus.

Photographs were also taken of the yielding patterns in the web and the buckling in the web and compression flange.

TABLE 2.1

TEST SPECIMENS

BEAM	SLAB WIDTH	LONGITUDINAL REINFORCEMENT	A_s (sq.in.)	A_s/A_{WF}	A_s/A_c	SHEAR CONNECTORS	TRANSVERSE REINFORCEMENT	A_t/A_c
11	4'-0"	6 #4 BARS	1.18	.111	.00615	3/4"ø x 3"@6"	#3 BARS @ 6"	.00468
12	4'-0"	10 #4 BARS	1.96	.185	.00995	3/4"ø x 3"@6"	#3 BARS @ 6"	.00468
13	4'-0"	8 #5 BARS	2.45	.232	.0128	3/4"ø x 3"@4½"	#3 BARS @ 4½"	.00605
14	4'-0"	12 #5 BARS	3.68	.348	.0192	7/8"ø x 3½"@4½"	#3 BARS @ 4½"	.00605
15	6'-0"	12 #5 BARS	3.68	.348	.0128	7/8"ø x 3½"@4½"	#3 BARS @ 4½"	.00605
16	2'-8"	8 #5 BARS	2.45	.232	.0192	3/4"ø x 3"@4½"	#3 BARS @ 4½"	.00605
17	6'-0"	8 #5 BARS	2.45	.232	.00850	3/4"ø x 3"@4½"	#3 BARS @ 4½"	.00605

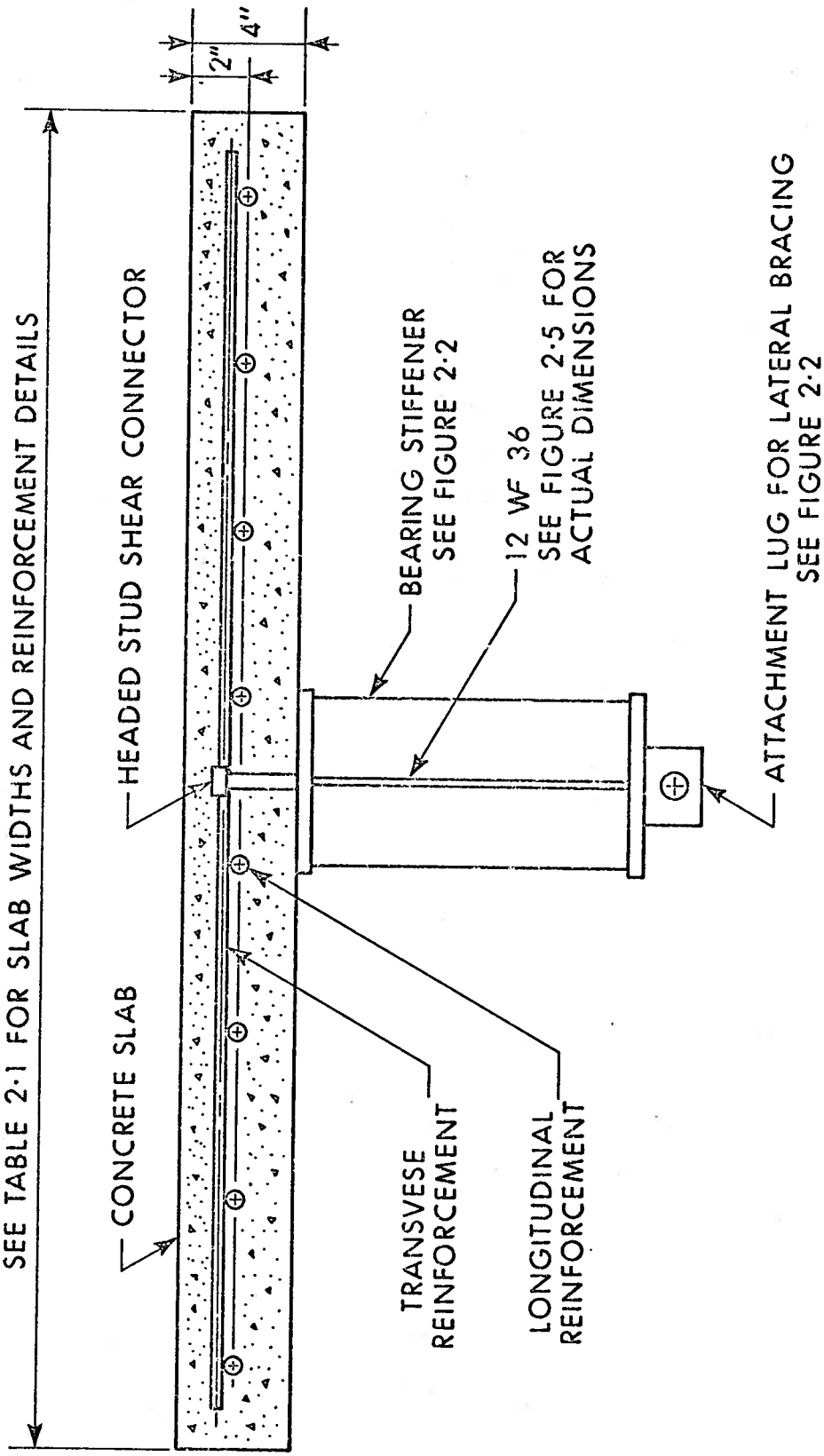

FIGURE 2·1 COMPOSITE BEAM CROSS SECTION

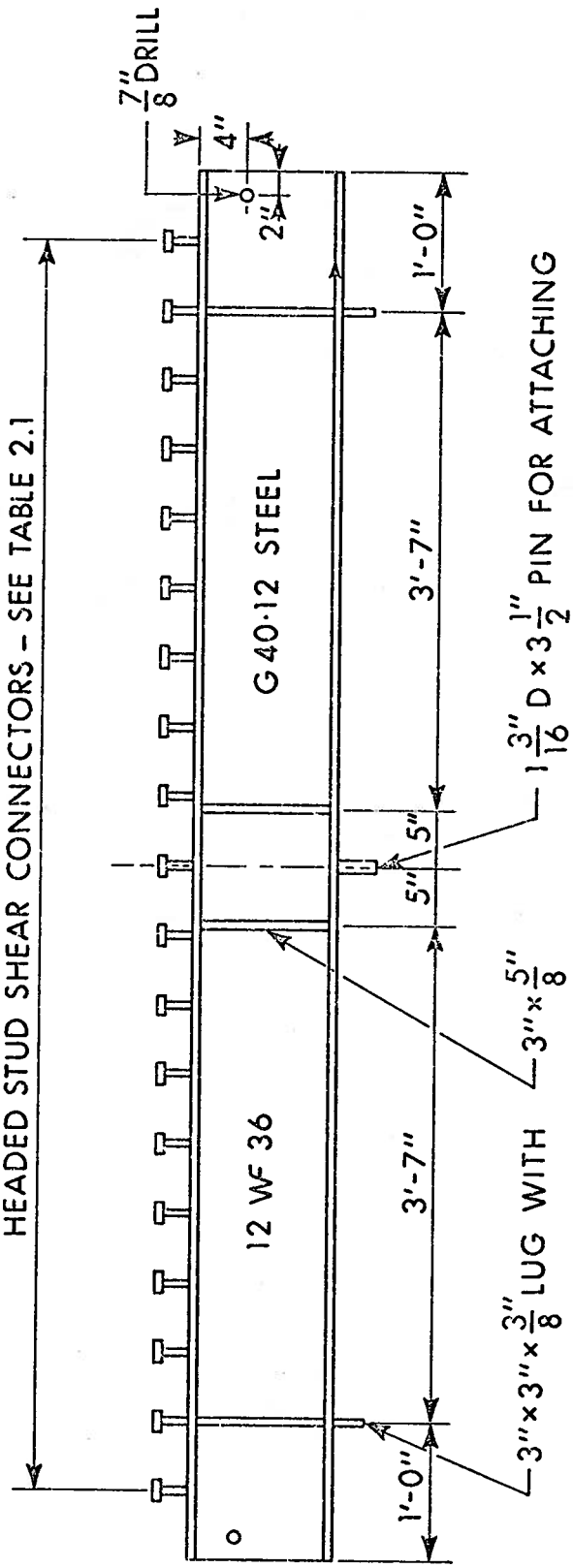

FIGURE 2.2 FABRICATED STEEL SECTION

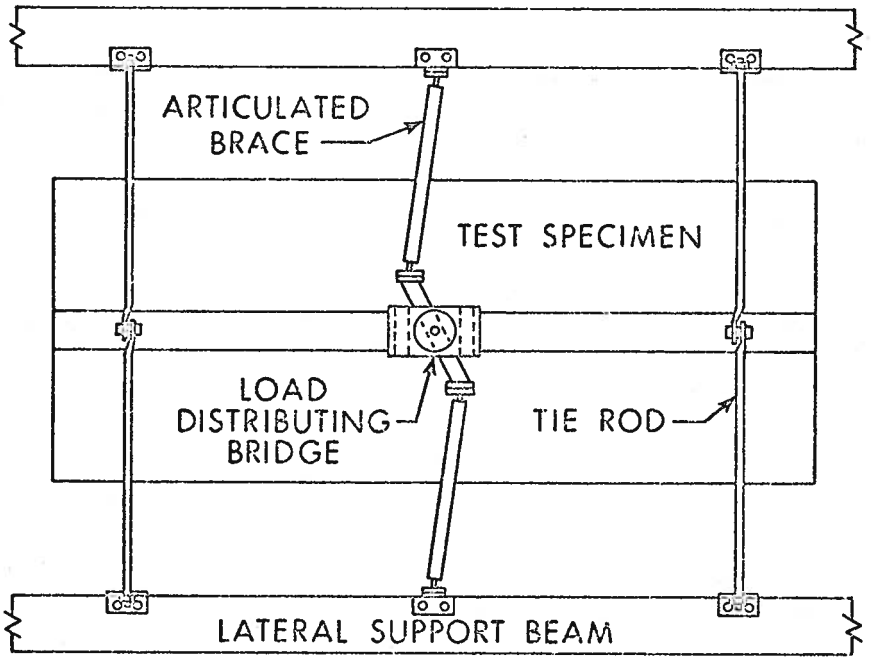

PLAN VIEW

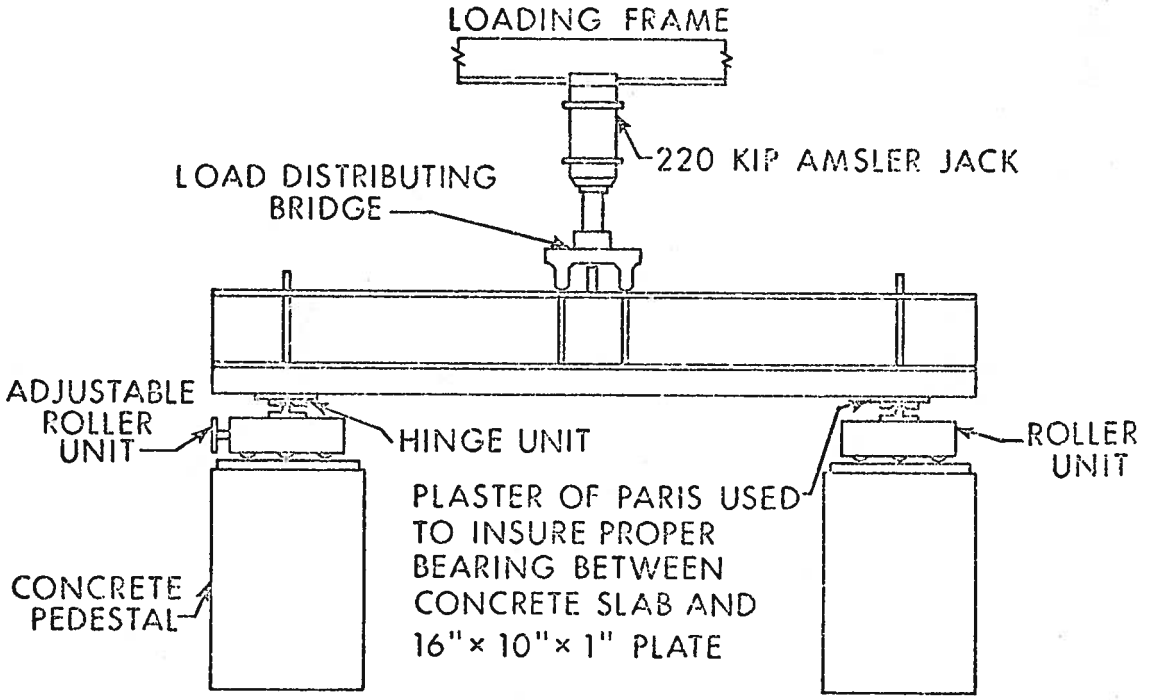

ELEVATION VIEW

FIGURE 2.3 TESTING APPARATUS

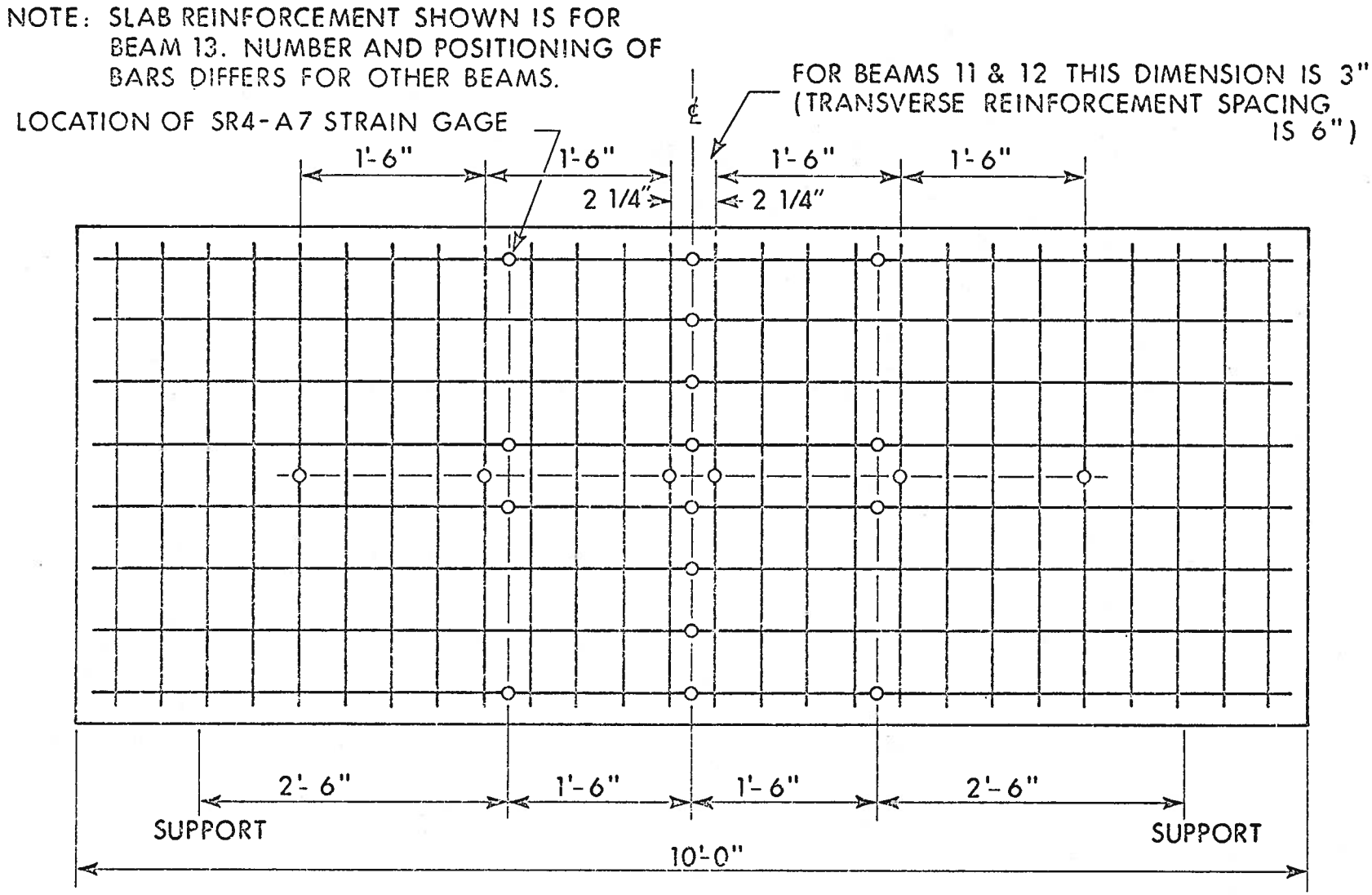

FIGURE 2.4 TYPICAL LOCATION OF STRAIN GAGES ON SLAB REINFORCEMENT

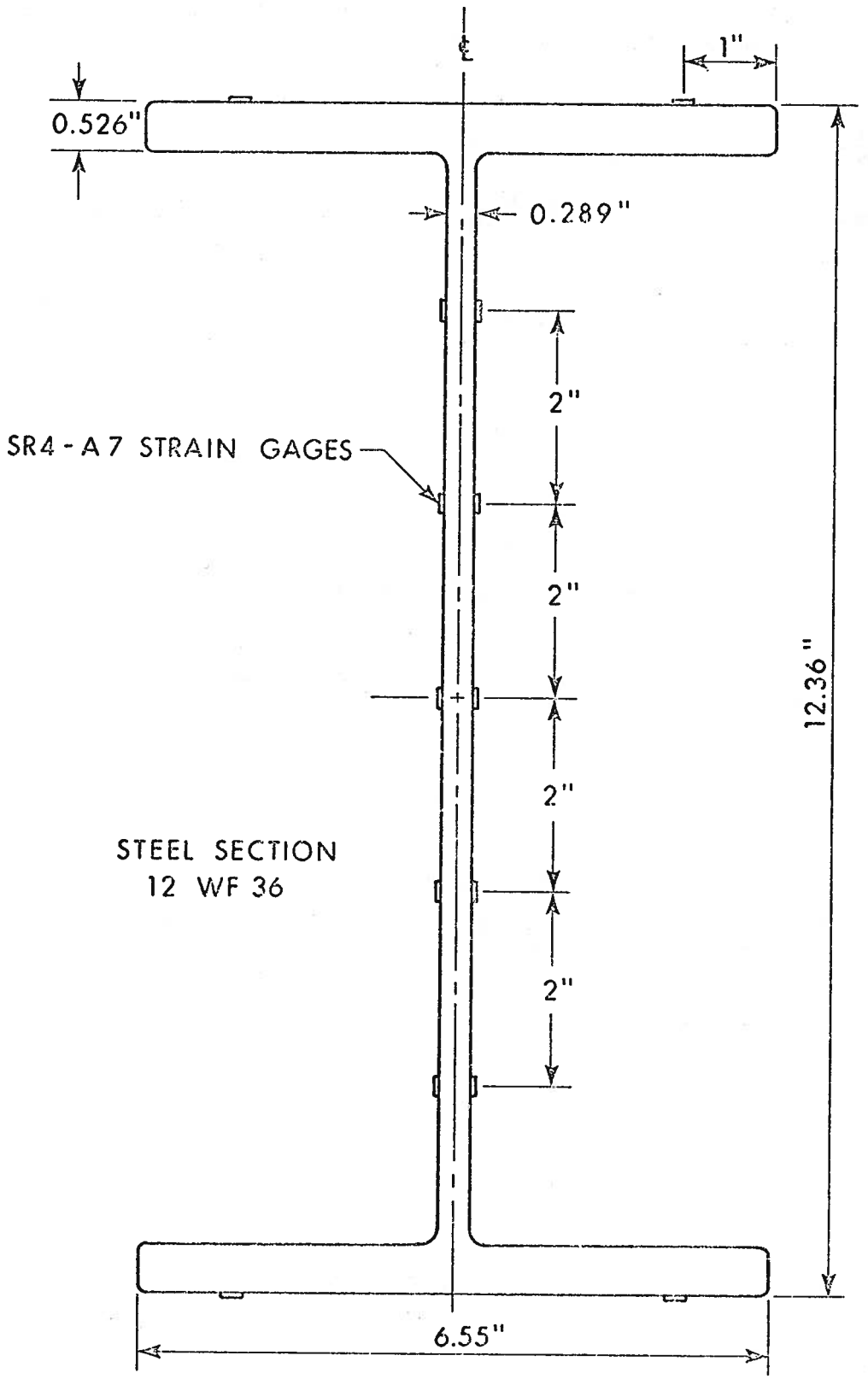

FIGURE 2.5 LOCATION OF STRAIN GAGES ON STEEL SECTION

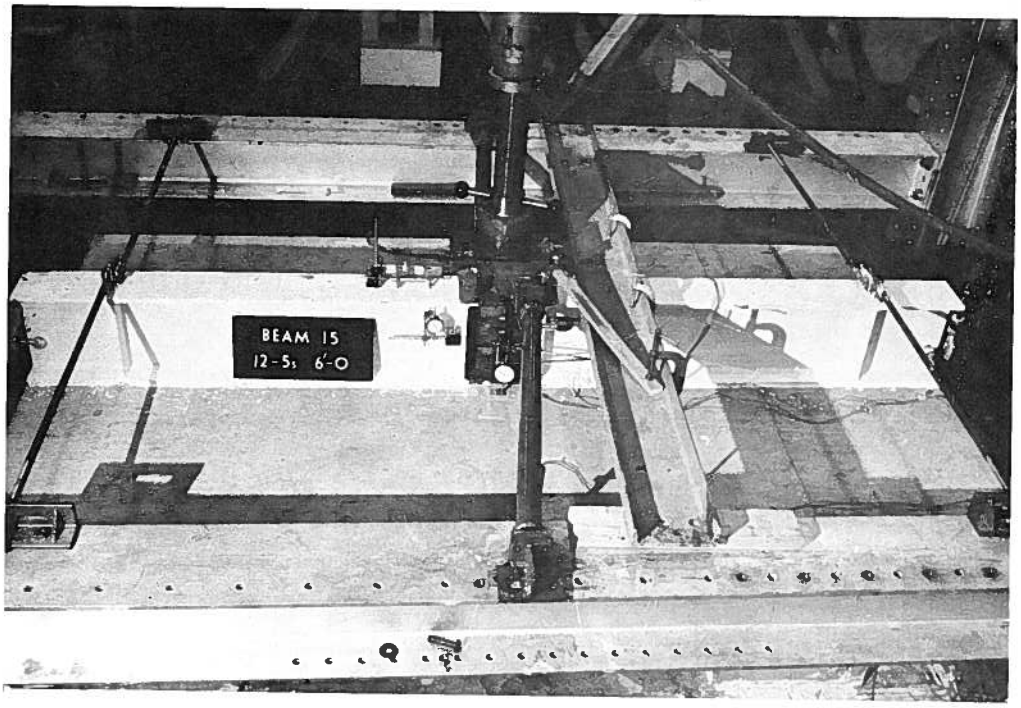

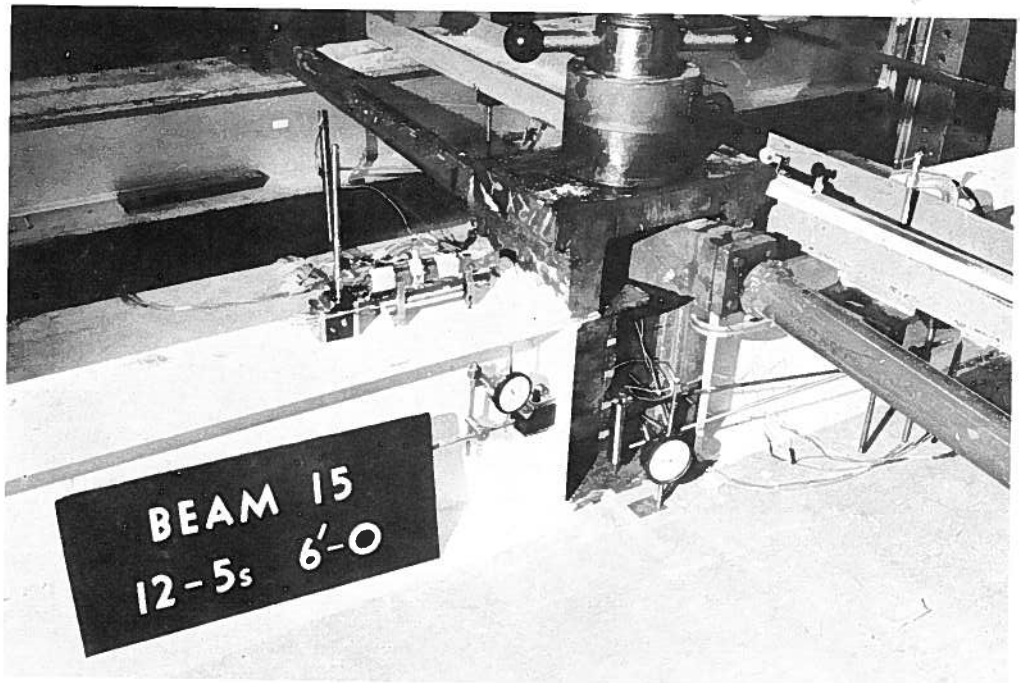

PLATE 2.1 TEST APPARATUS

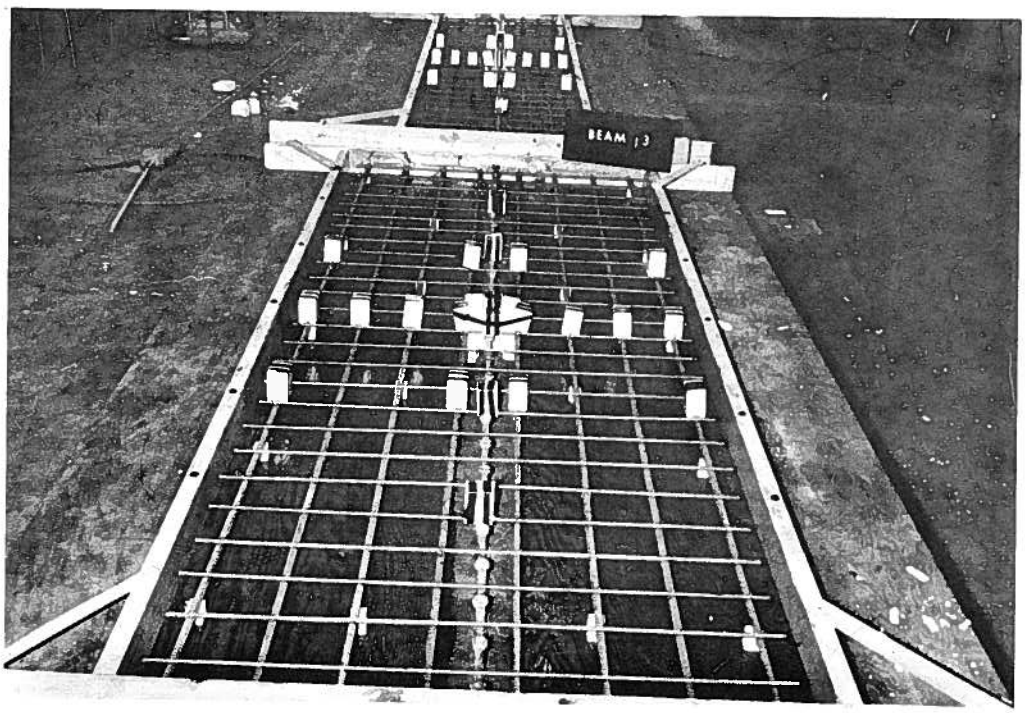

PLATE 2.2 SPECIMEN PRIOR TO CASTING

CHAPTER III

TEST RESULTS

3.1 INTRODUCTION

All original data obtained from the beam tests is filed with the Department of Civil Engineering, University of Alberta. Much of the test data is presented herein, principally in graphical and tabular form.

3.2 GENERAL BEHAVIOR

The behavior of all the test beams under increasing load was essentially the same. At low loads midspan deflection increased slowly in direct proportion to the load. Deflections increased more rapidly as the midspan moment approached the plastic moment value. As further load was applied, additional rotation of the specimen became concentrated at midspan as is expected in a beam under high moment gradient. Each beam continued to take additional load well beyond its simple plastic load. Finally a local buckle developed in the compression portion of the web, followed by local buckling of the compression flange. At this point the specimen began to gradually unload while continuing to deflect until lateral buckling of the compression flange occurred. The test was terminated when the loading jack ran out of travel. Views of typical local buckles and yield patterns in the web are shown in PLATES 3.1 and 3.2 respectively.

3.3 LOAD-DEFLECTION RELATIONSHIPS

FIGURE 3.1 presents the load-deflection curves for Beams 11, 12, 13 and 14, the test specimens with varying amounts of longitudinal slab reinforcement and a constant slab width of 4'-0". Beam 18, the WF section only, is shown for comparison. FIGURE 3.2 presents the load-deflection curves for Beams 13, 14, 15, 16 and 17, the test beams with varying slab widths and varying ratios of longitudinal reinforcement to area of concrete. Each deflection value plotted represents the average reading of two displacement transducers positioned on the tension flange of the test beam, one on each side of the web.

3.4 MOMENT-CURVATURE RELATIONSHIPS

The relationships between bending moment and curvature at midspan are shown in FIGURES 3.3, 3.4, 3.5 and 3.6. Curvatures were determined from plots of the strain distribution across the WF section. FIGURE 3.3 presents the moment-curvature relationships for Beams 11, 12, 13, 14 and 18, while FIGURE 3.4 presents the curves for Beams 13, 14, 15, 16 and 17. In FIGURES 3.5 and 3.6 the ratio of moment to computed simple plastic moment capacity (M/M_p) is used to non-dimensionalize the moment scale. The test specimens are again divided into two groups as above.

3.5 LONGITUDINAL REINFORCEMENT STRAINS AT MIDSPAN

Distributions of longitudinal reinforcement strains at midspan across the concrete slab are shown in FIGURES 3.7, 3.8, and 3.9 for the different test beams. Each point represents the average

strain in two bars symmetrically positioned.

3.6 TRANSVERSE BENDING OF THE CONCRETE SLAB

FIGURE 3.10 shows the comparison of edge and centreline deflections at midspan for each of the test specimens. Relative deflection is defined as centreline deflection minus edge deflection. Thus for a beam tested with its slab on the underside a positive relative deflection corresponds to a curl of the edges toward the steel section. In calculating relative deflections, the edge and centreline deflections were each determined as average values obtained from two displacement transducers.

Values of the strain in the transverse slab reinforcement at midspan are given in FIGURE 3.11 for each test beam. All such values represent the average of the strains in the two transverse bars positioned nearest to midspan.

3.7 CRACKING OF THE CONCRETE SLAB

The crack patterns in the concrete slabs are shown in PLATES 3.3, 3.4 and 3.5. The position of the numbers indicate the extent of the crack at different load increments. At low loads transverse cracking occurred, first along planes weakened by the voids placed in the concrete for the placement of strain gages. As the load increased these cracks grew wider and additional transverse cracking occurred. Diagonal cracks developed across the slab as failure approached.

3.8 ULTIMATE LOAD CONDITIONS

Values of ultimate moment and theoretical plastic moment capacity are compared in TABLE 3.1. The variation in M_{ult}/M_p with respect to the total tensile force in the longitudinal slab reinforcement at yield ($A_s f_y$) is shown in FIGURE 3.12. The ratio of ultimate moment of the composite section to the ultimate moment of the WF section alone is shown in FIGURE 3.13 as a function of the tensile force in the longitudinal slab reinforcement at yield. The increase in simple plastic moment capacity is plotted for comparison.

Rotation capacity at ultimate moment is shown in a non-dimensionalized plot of M_{ult}/M_p versus ϕ_{ult}/ϕ_p' in FIGURE 3.14. Definition of the above terms is shown in the inset on the figure. ϕ_p' was taken as 0.000240 radians per inch for all the beams tested. Values from the negative bending tests of Piepgrass[1] and the positive bending tests of Ferrier[8] are included in the figure.

3.9 INTERACTION BETWEEN WF SECTION AND LONGITUDINAL SLAB REINFORCEMENT

The "interaction factor" between the WF section and the longitudinal slab reinforcement is defined as the ratio of measured strain in the reinforcement to the calculated strain at the level of the reinforcement obtained as a projection from the strain distribution across the WF section. TABLE 3.2 presents values of these interaction factors at ϕ_p' and at the yield strain of the reinforcement.

TABLE 3.1

TEST RESULTS

BEAM	P_{ult} (kips)	M_{ult} (ft. kips)	M_p (ft. kips)	M_{ult}/M_p	M_{ult}/M^o_{ult}	M_p/M^o_p
11	156	279.6	207.6	1.347	1.156	1.222
12	160	286.7	225.0	1.274	1.185	1.324
13	162	290.3	231.3	1.255	1.200	1.361
14	164	293.9	245.3	1.198	1.215	1.444
15	166	297.5	245.3	1.213	1.230	1.444
16	161	288.5	231.3	1.247	1.193	1.361
17	160	286.7	231.3	1.240	1.185	1.361
18	135	241.9	169.9	1.424	1.000	1.000

TABLE 3.2

INTERACTION BETWEEN WF SECTION AND

LONGITUDINAL SLAB REINFORCEMENT

BEAM	INTERACTION FACTOR	
	AT ϕ'_p	AT YIELD OF LONGITUDINAL REINFORCEMENT
11	1.29	1.40
12	0.69	0.64
13	0.66	0.62
14	0.64	0.42
15	0.56	0.51
16	0.51	0.49
17	0.73	0.57

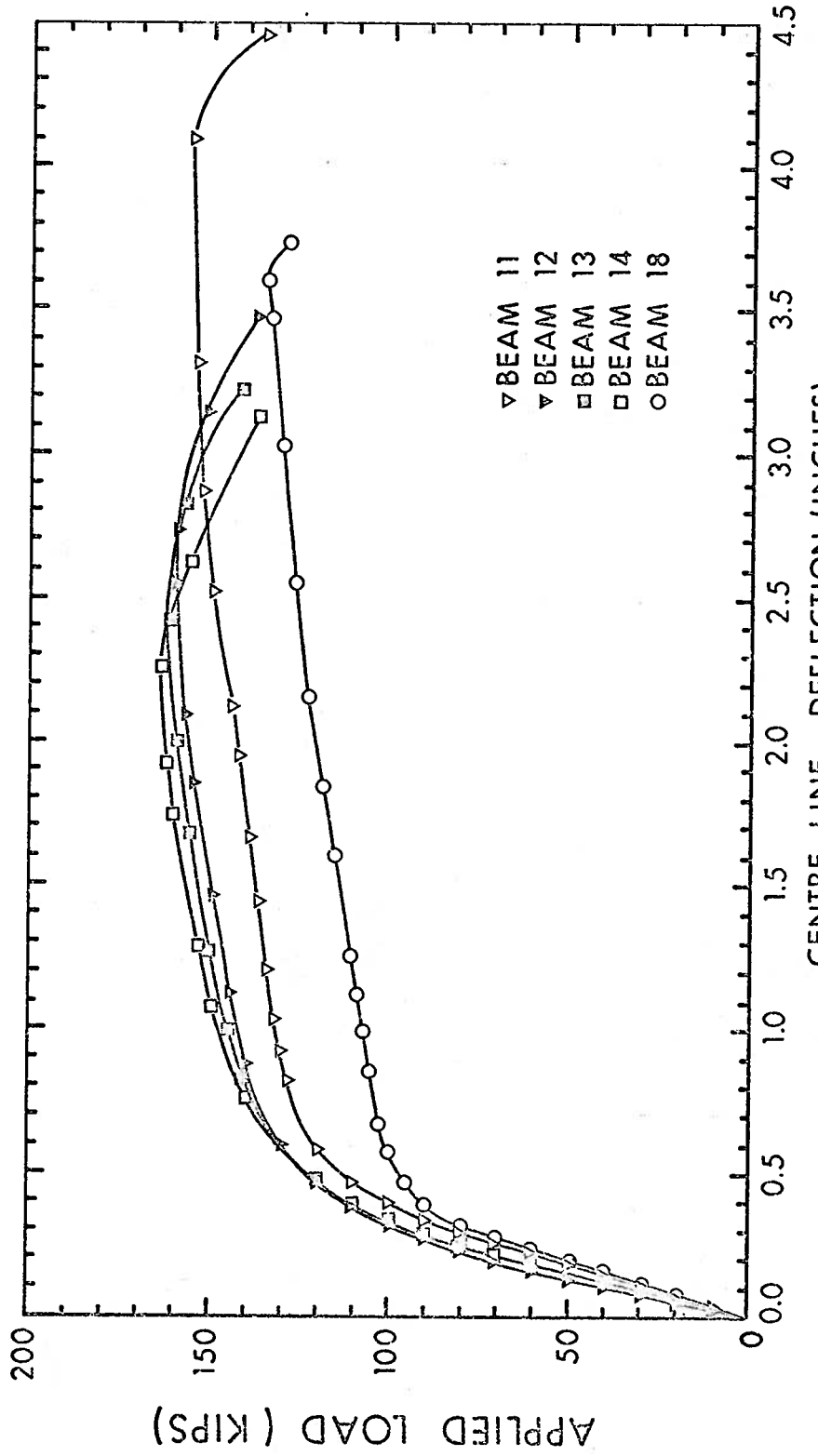

FIGURE 3.1 LOAD - DEFLECTION RELATIONSHIPS

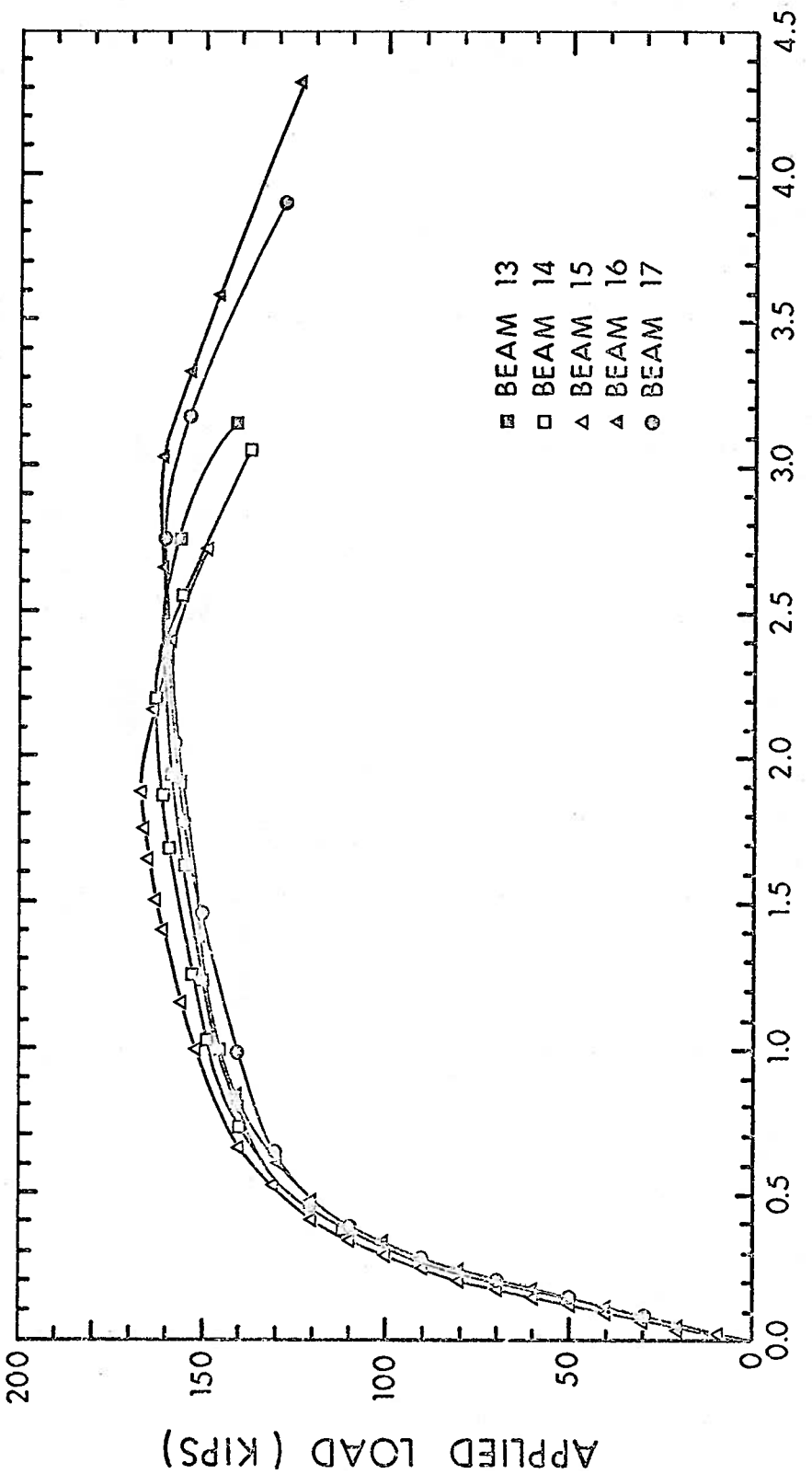

FIGURE 3.2 LOAD - DEFLECTION RELATIONSHIPS

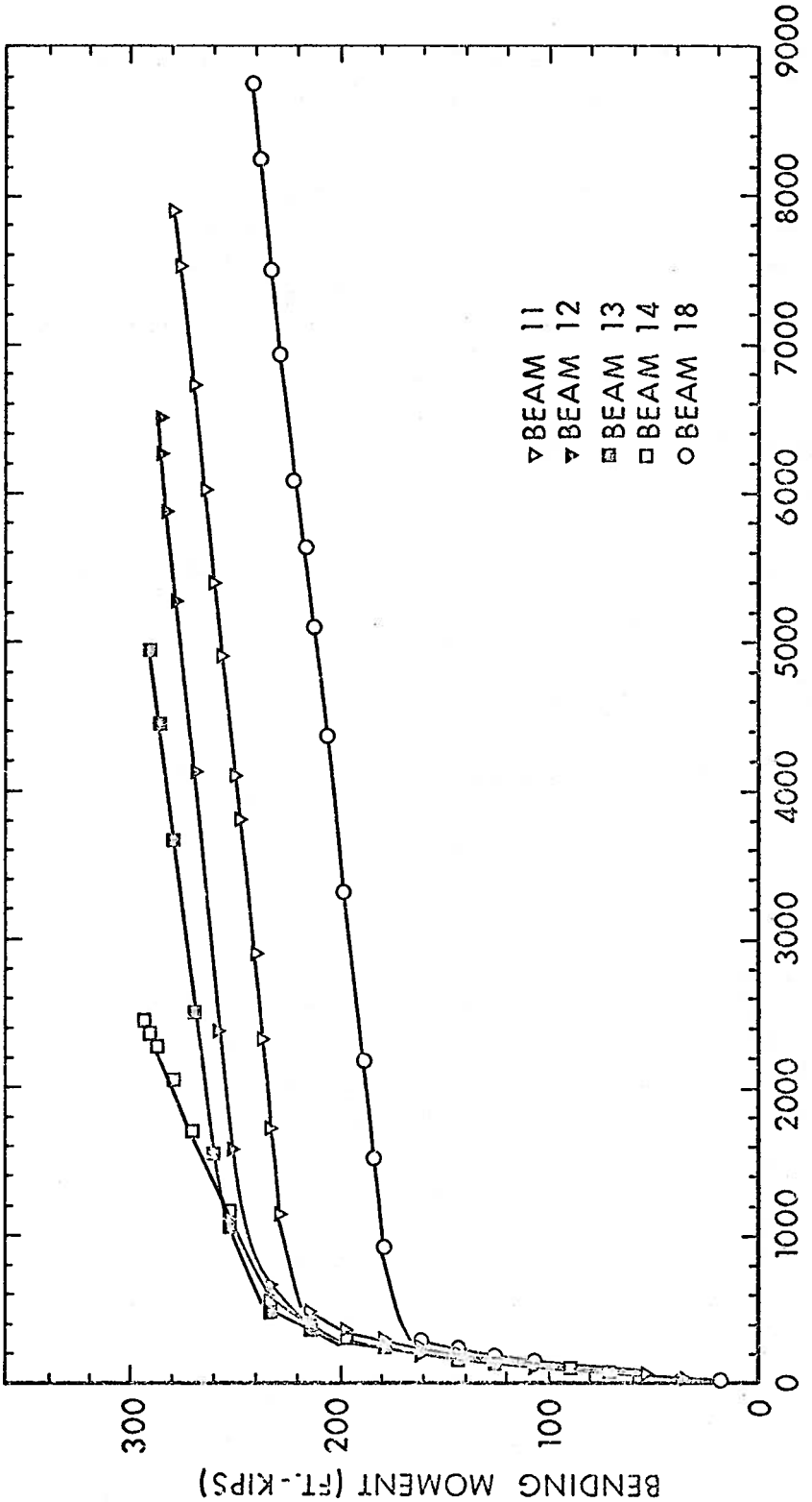

FIGURE 3.3 MOMENT – CURVATURE RELATIONSHIPS

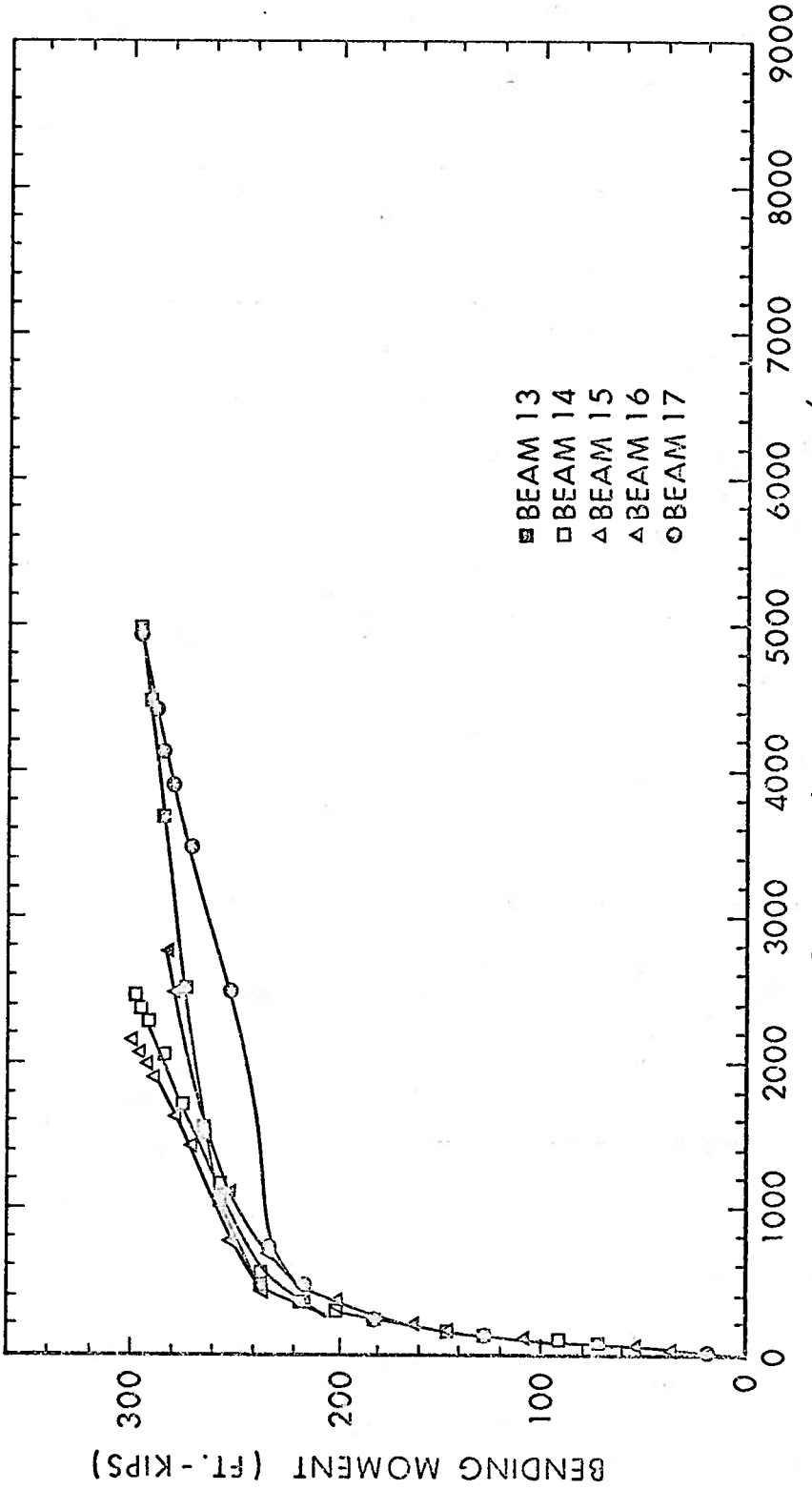

FIGURE 3·4 MOMENT-CURVATURE RELATIONSHIPS

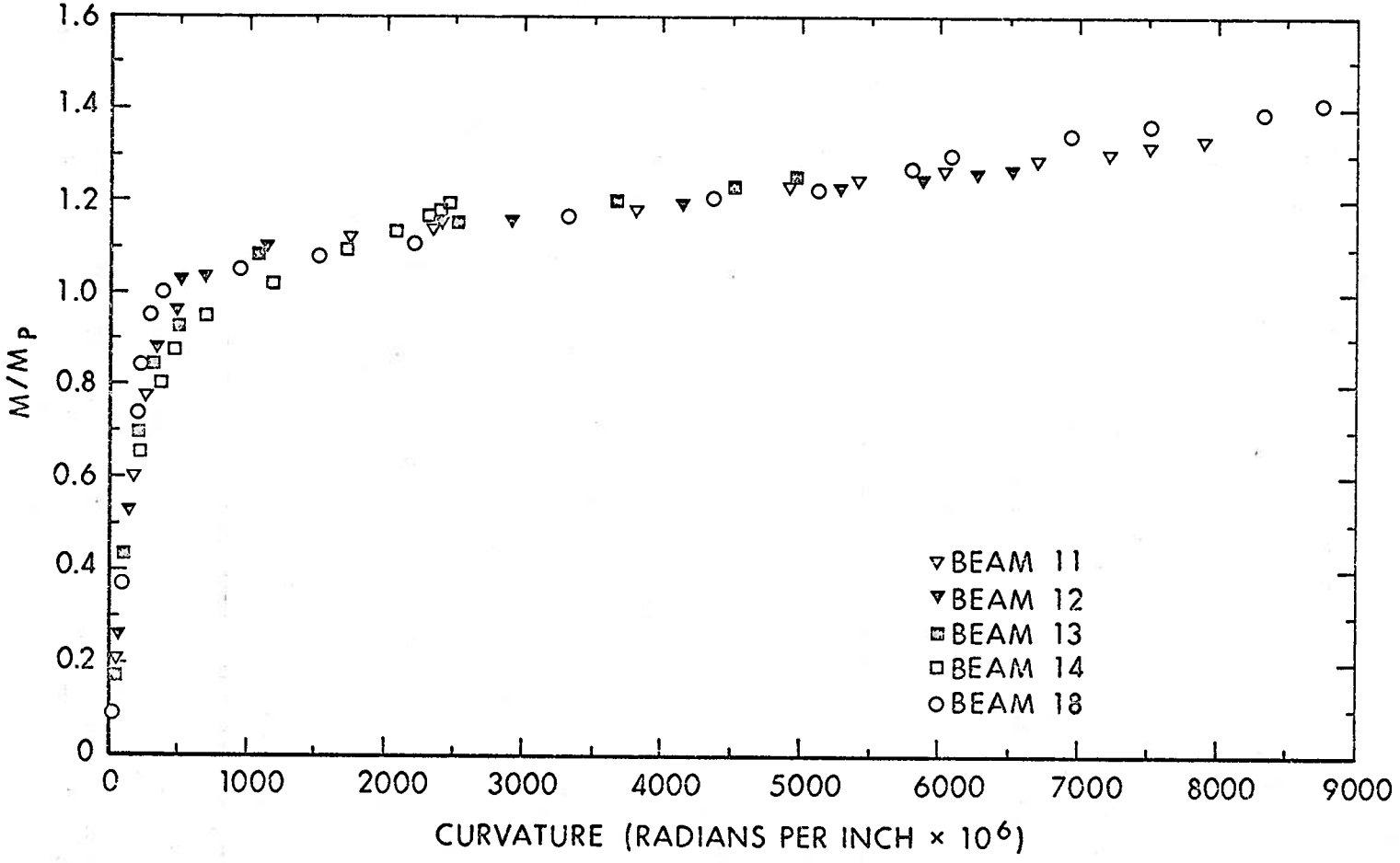

FIGURE 3.5 MOMENT CURVATURE RELATIONSHIPS

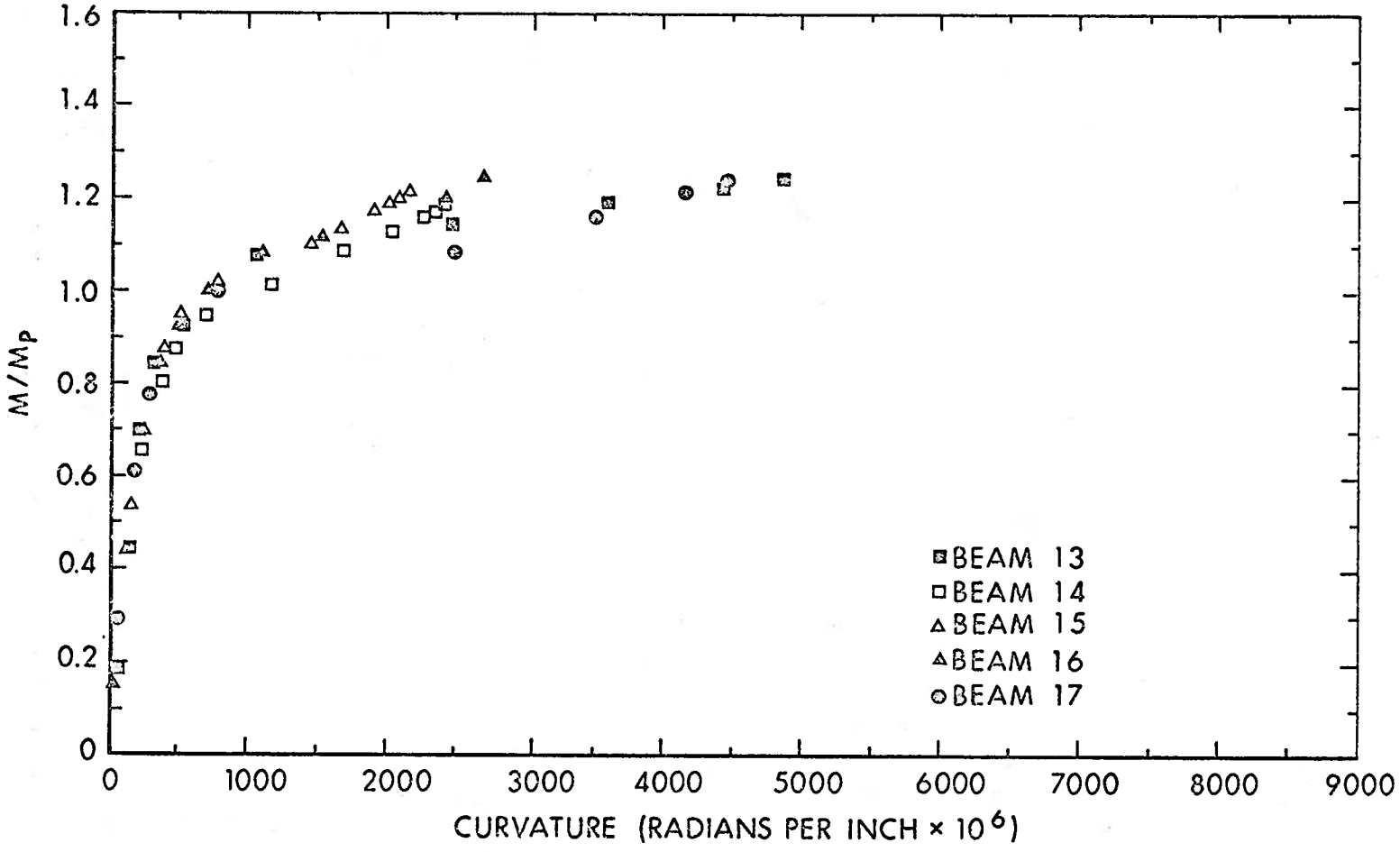

FIGURE 3.6 MOMENT-CURVATURE RELATIONSHIPS

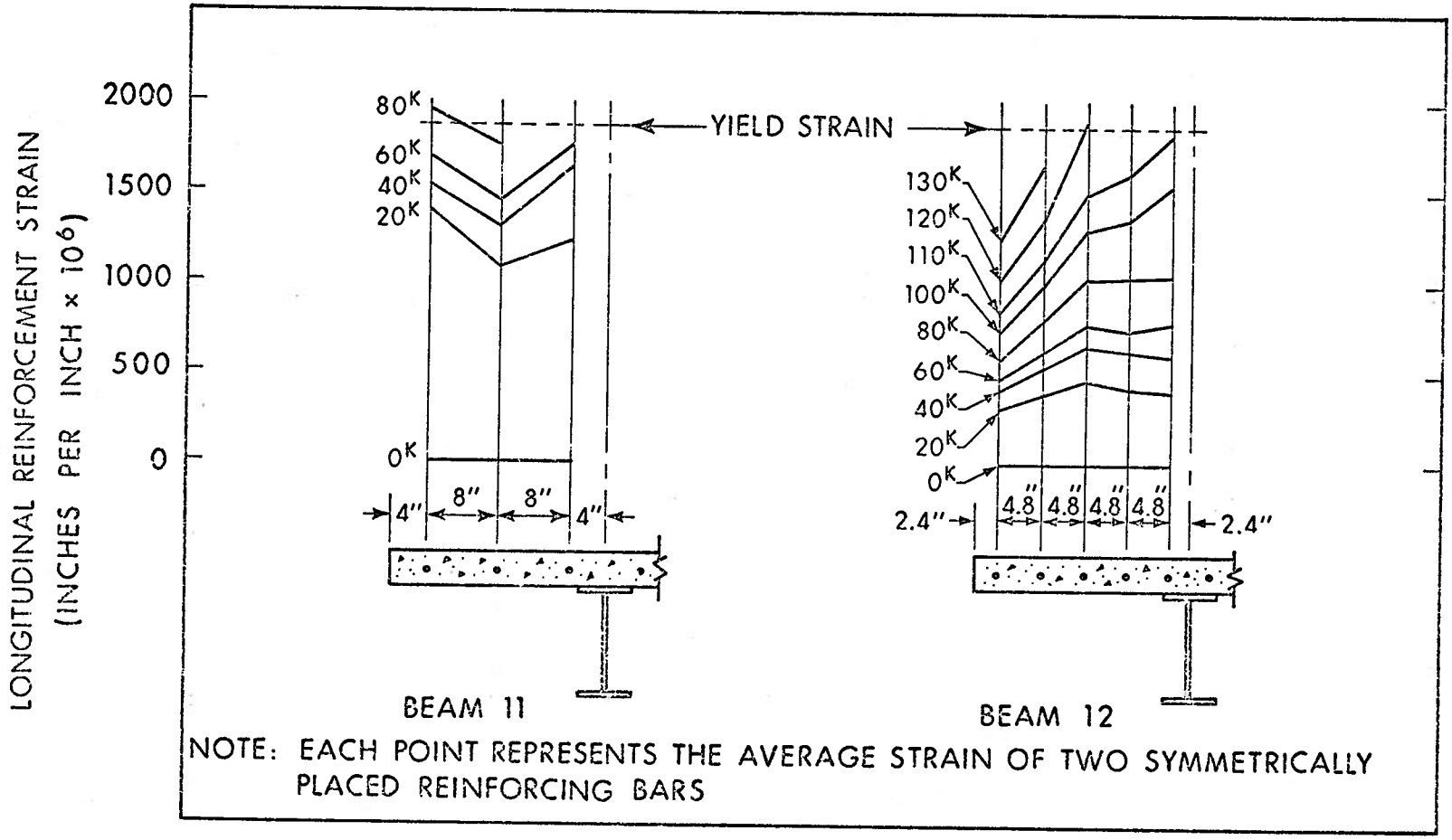

FIGURE 3.7 LONGITUDINAL REINFORCEMENT STRAINS AT MIDSPAN

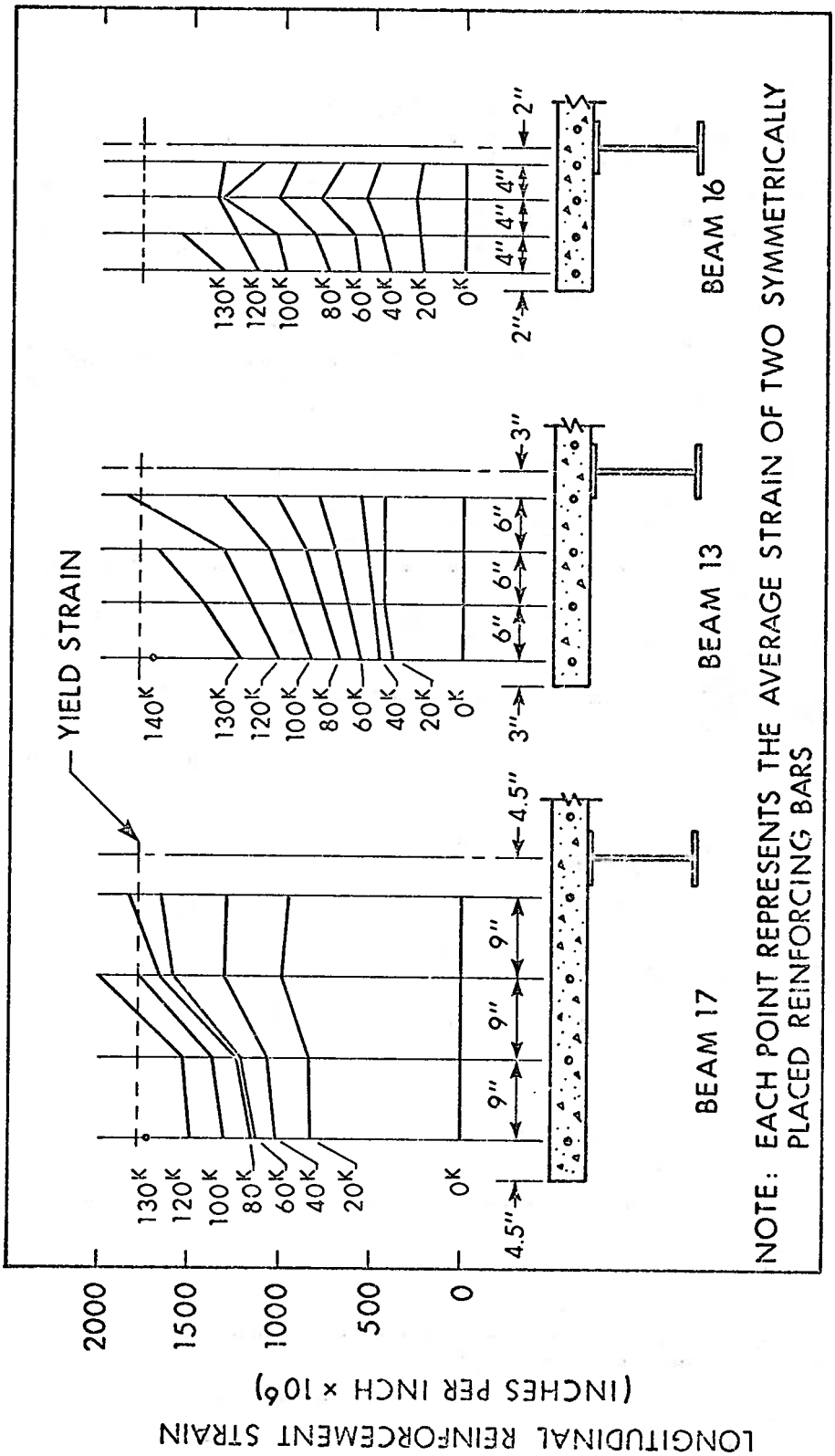

FIGURE 3.8 LONGITUDINAL REINFORCEMENT STRAINS AT MIDSPAN

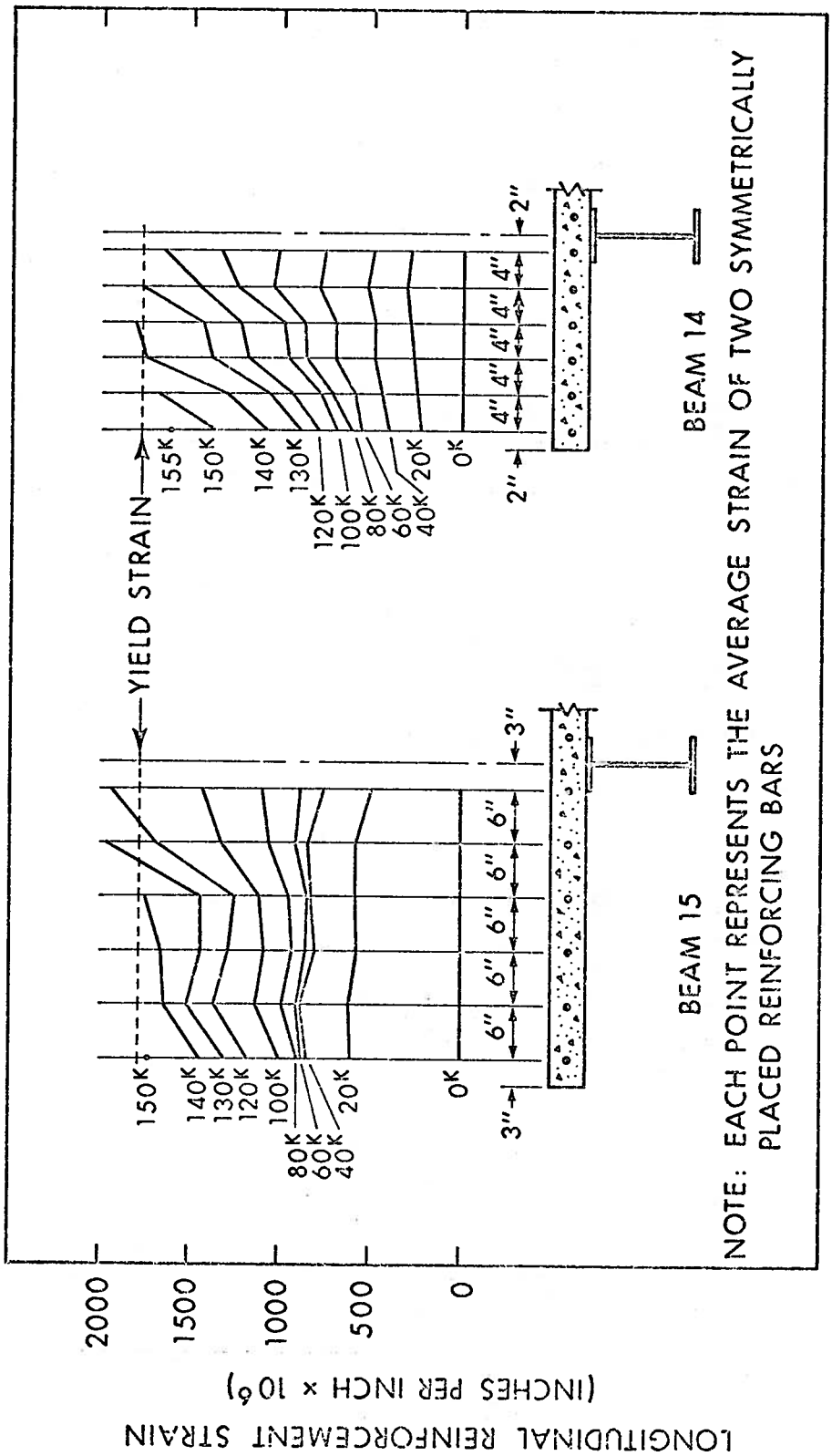

FIGURE 3.9 LONGITUDINAL REINFORCEMENT STRAINS AT MIDSPAN

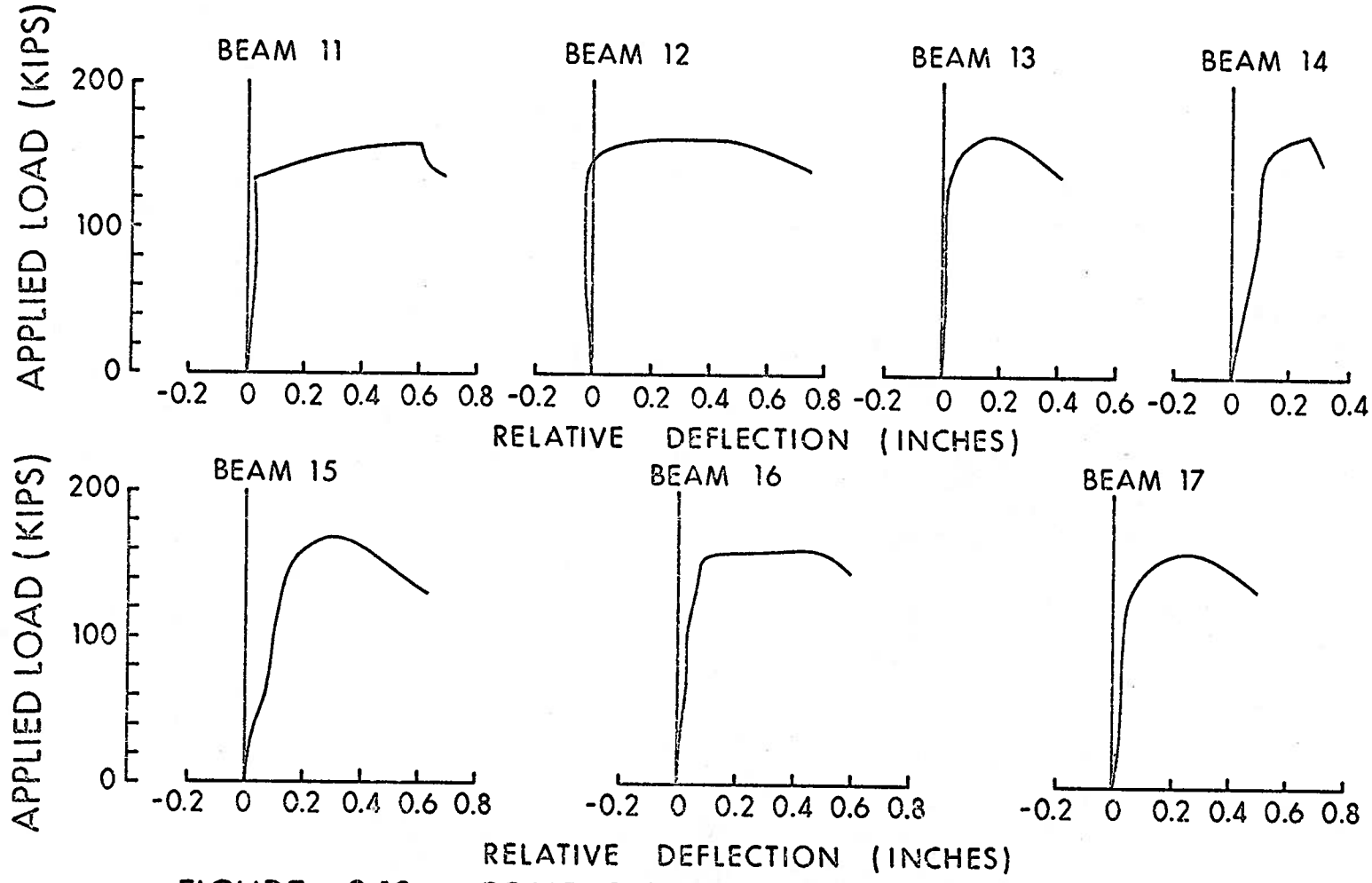

FIGURE 3.10 COMPARISON OF EDGE AND CENTRELINE DEFLECTIONS AT MIDSPAN

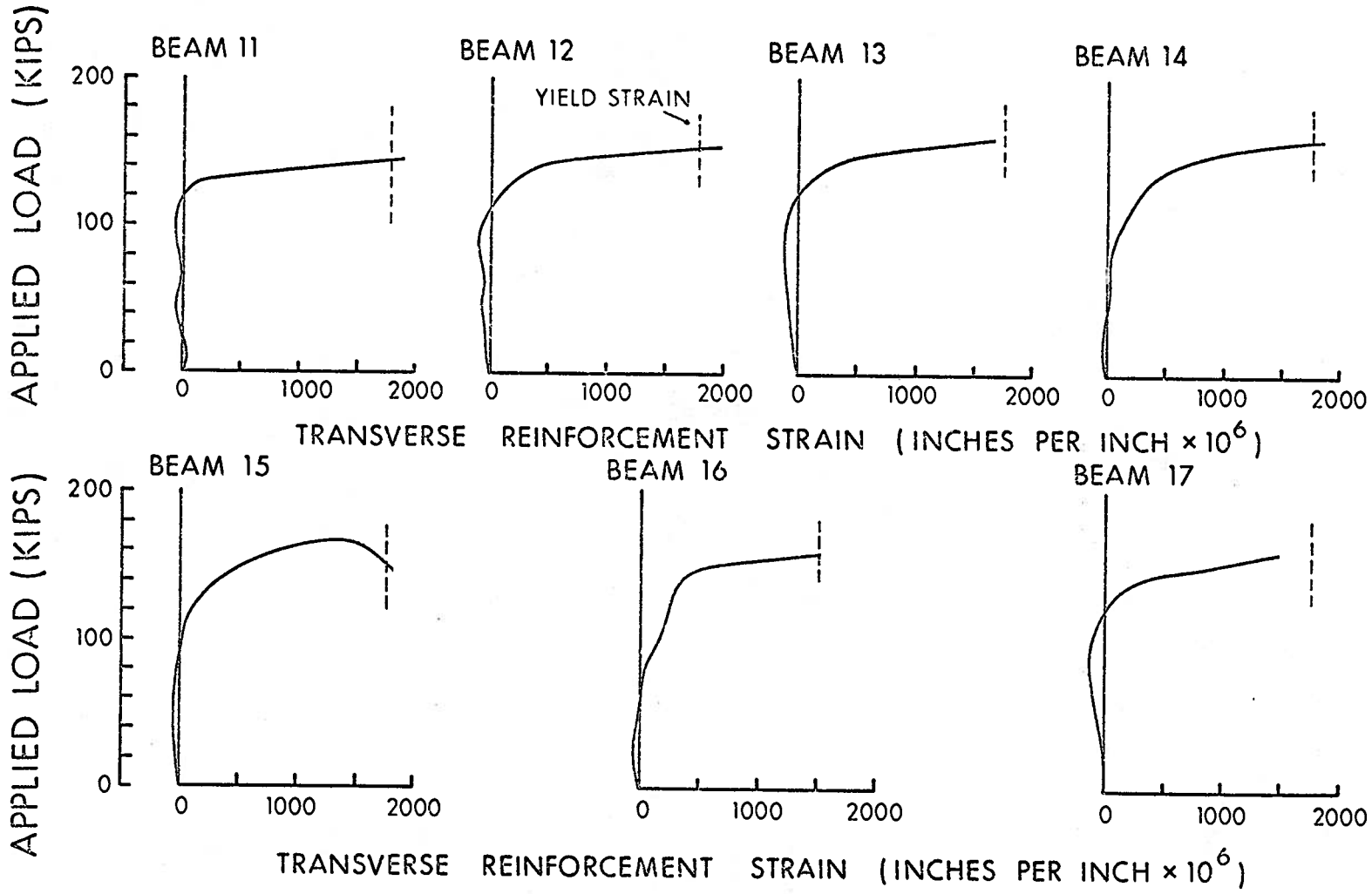

FIGURE 3.11 MIDSPAN TRANSVERSE REINFORCEMENT STRAINS

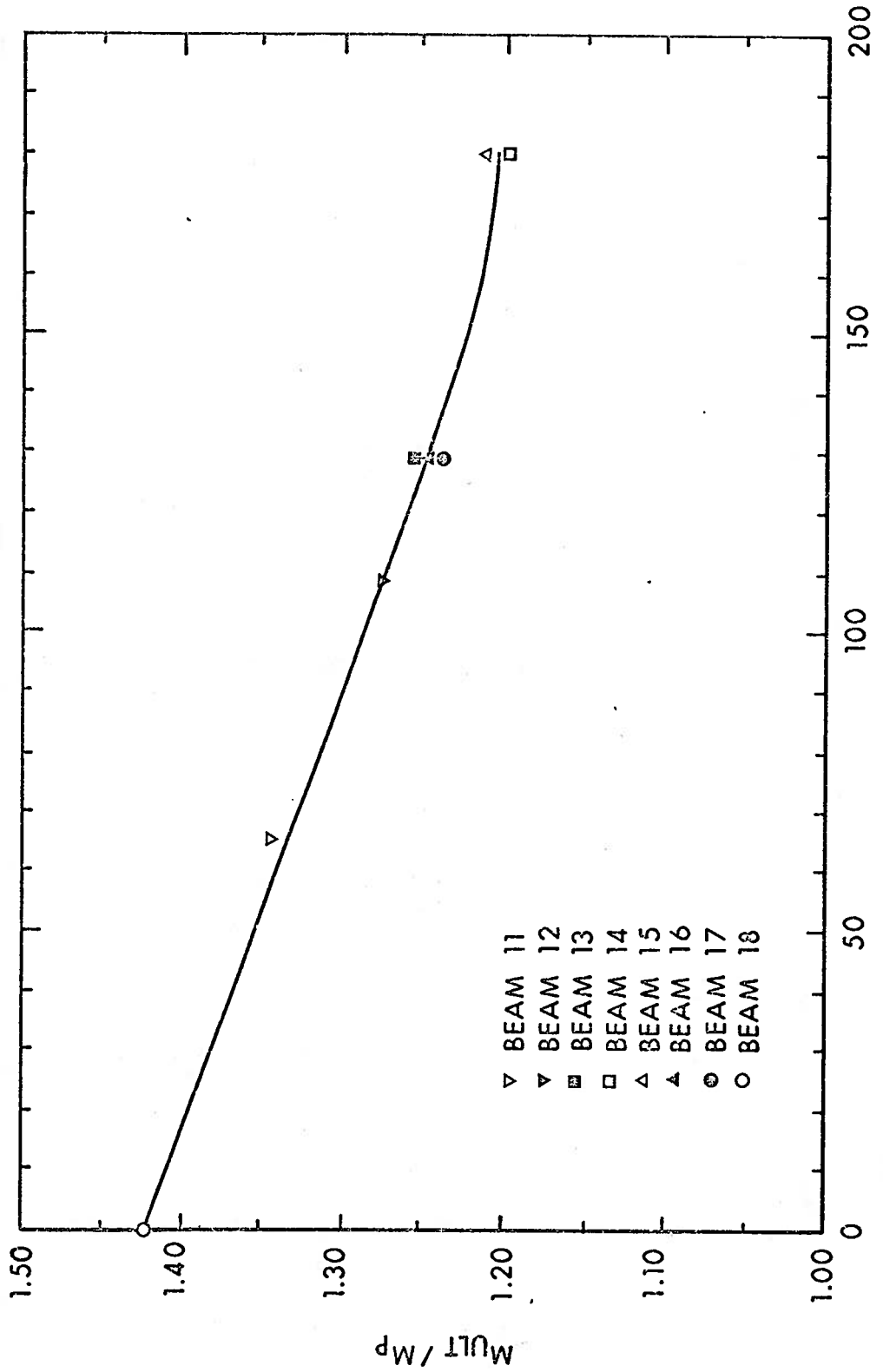

FIGURE 3.12 VARIATION OF M_{ULT}/M_p WITH INCREASING SLAB REINFORCEMENT

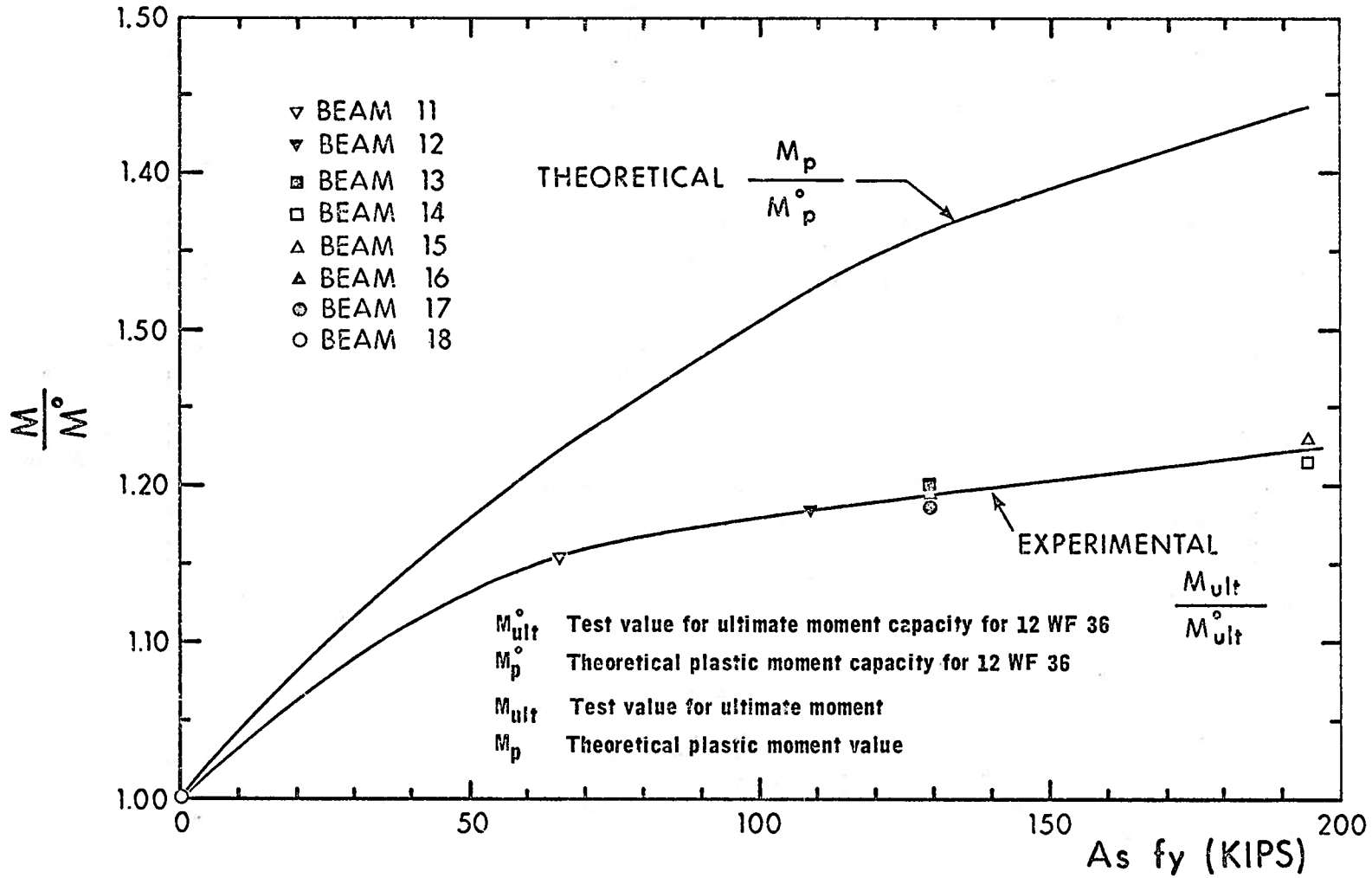

FIGURE 3.13 INCREASE IN MOMENT CAPACITY DUE TO LONGITUDINIAL REINFORCEMENT

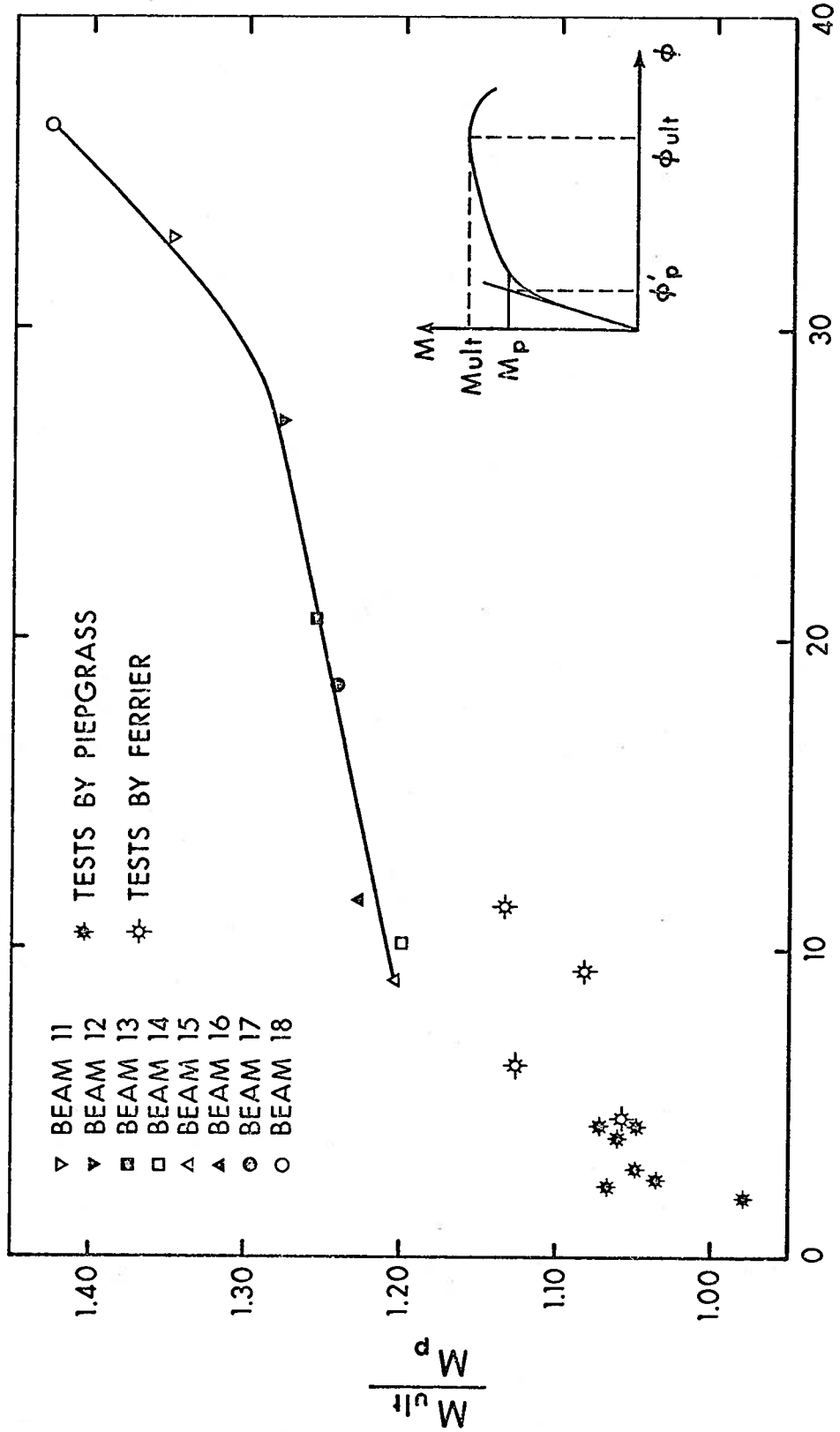

FIGURE 3.14 ROTATION CAPACITY AT ULTIMATE MOMENT ϕ_{ult}/ϕ'_p

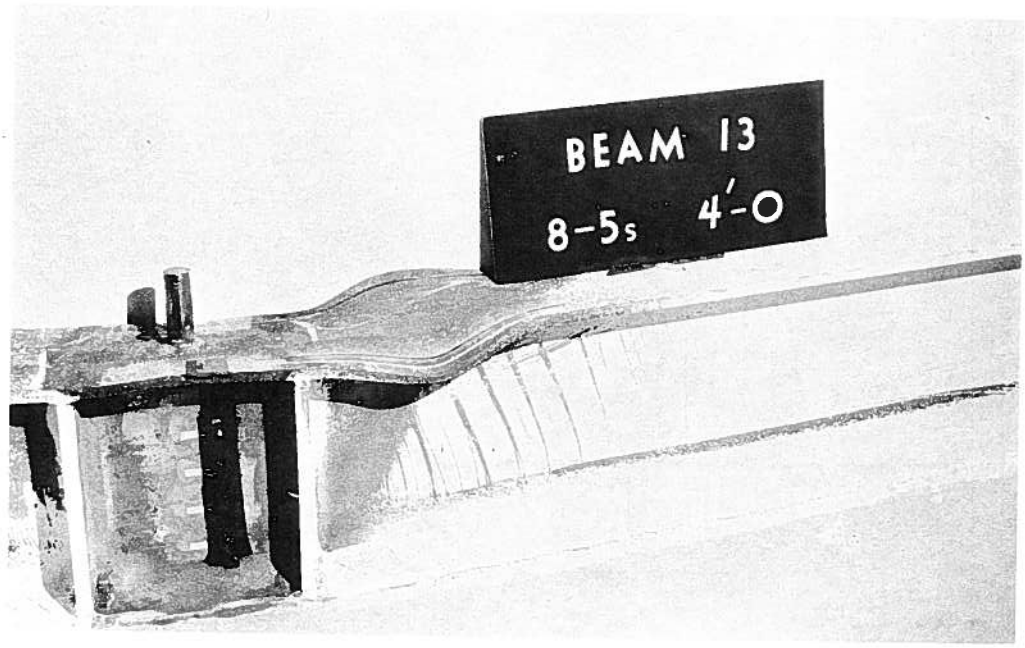

PLATE 3.1 TYPICAL LOCAL BUCKLES

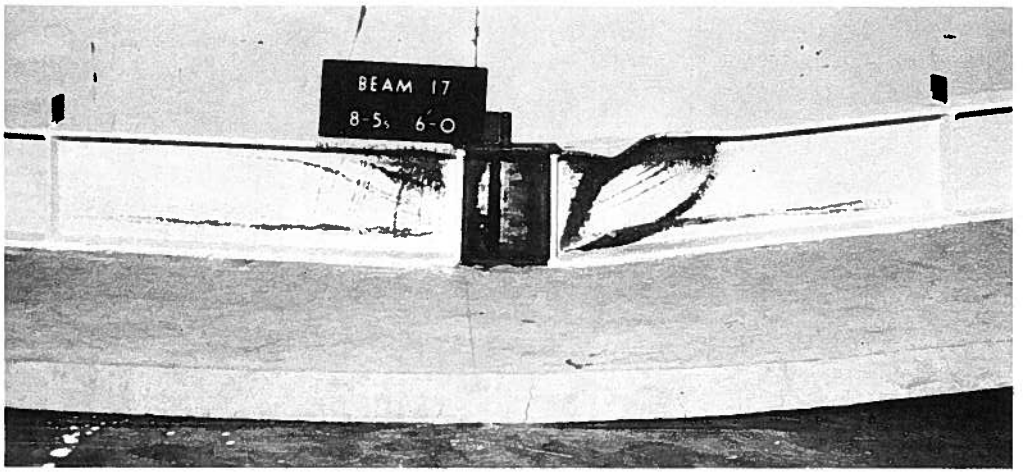

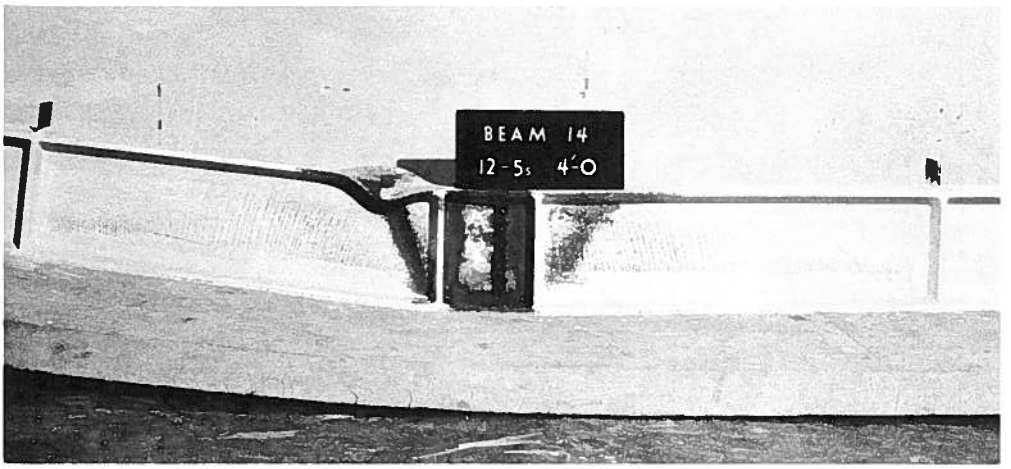

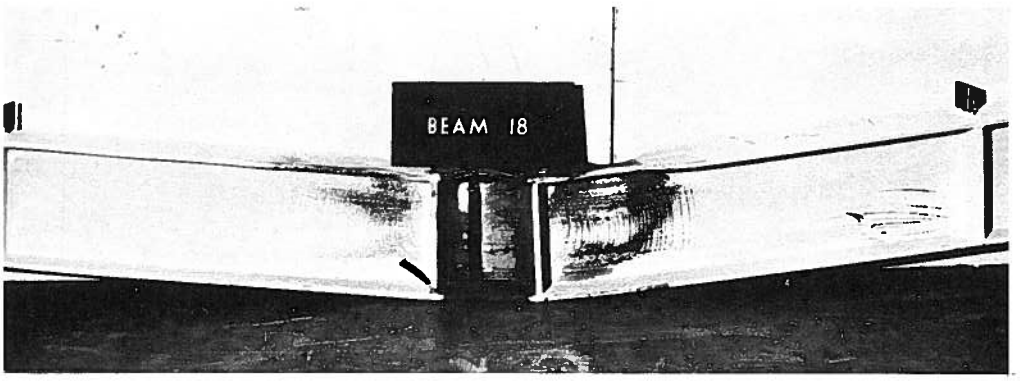

PLATE 3.2 YIELD PATTERNS IN WEB

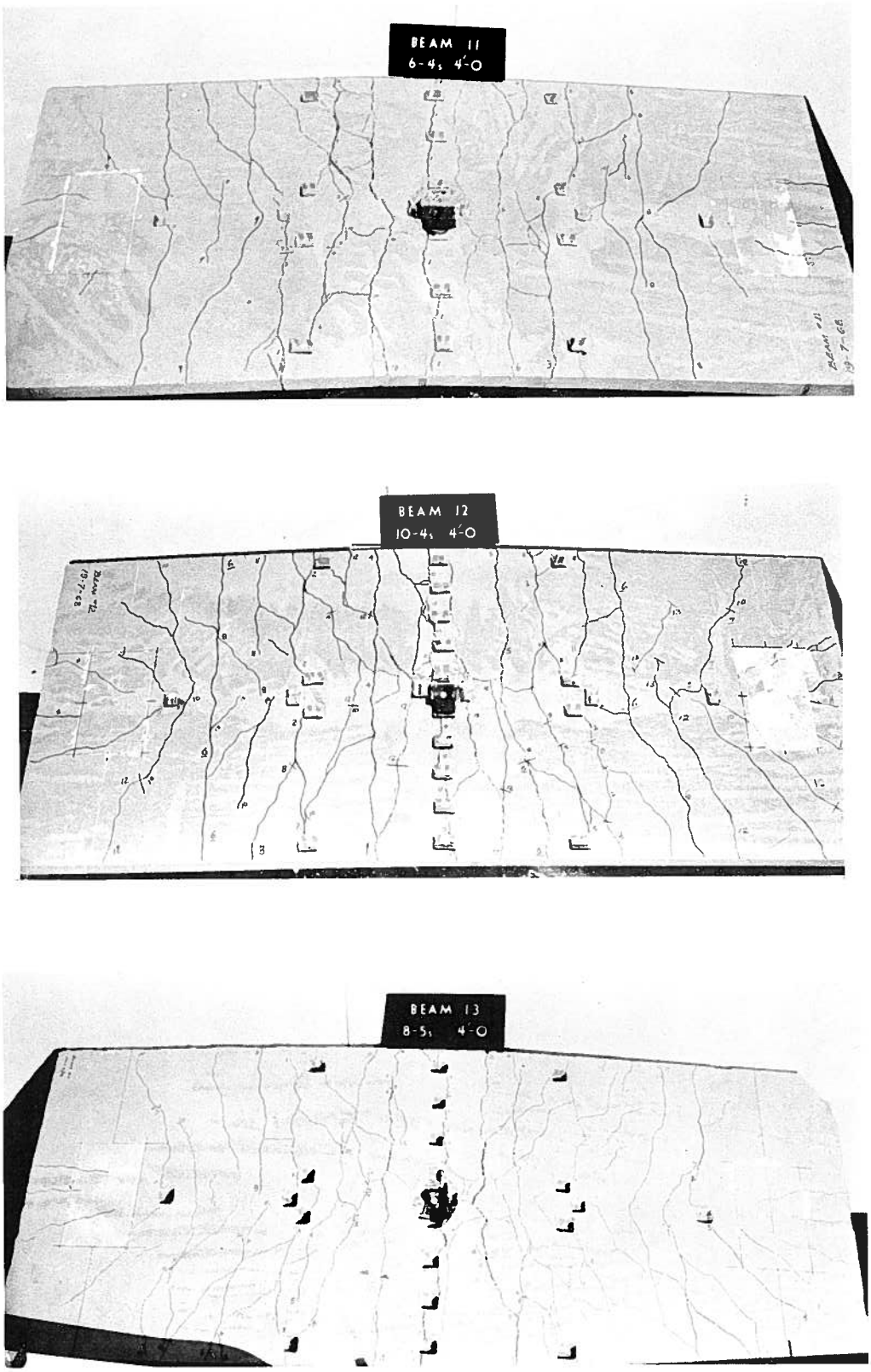

PLATE 3.3 CRACK PATTERNS

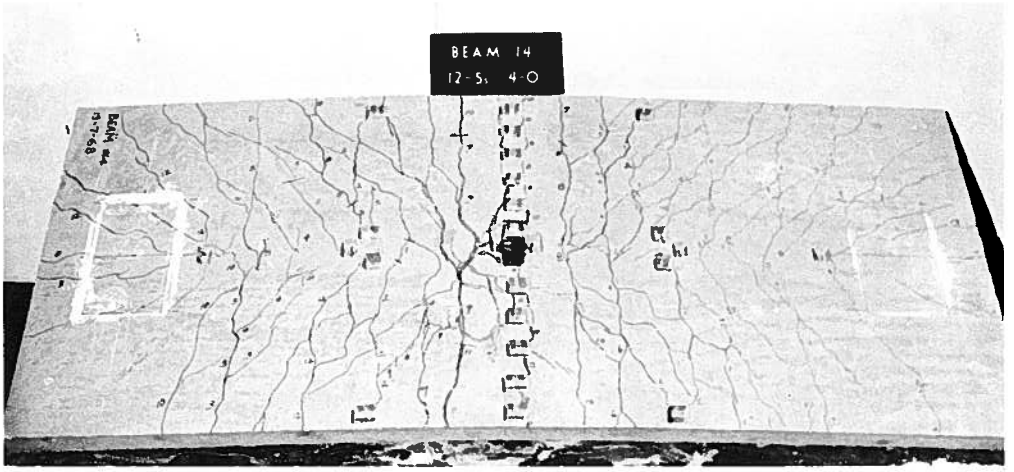

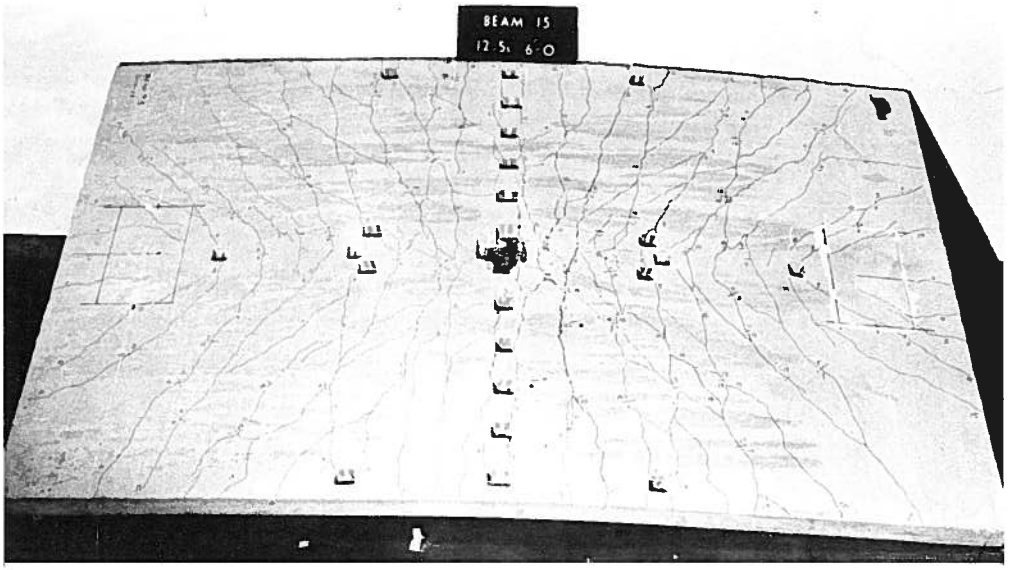

PLATE 3.4 CRACK PATTERNS

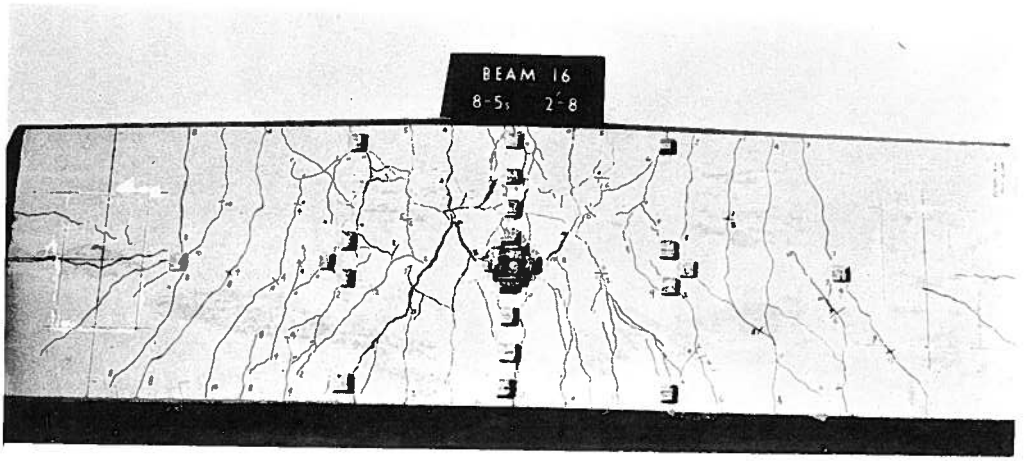

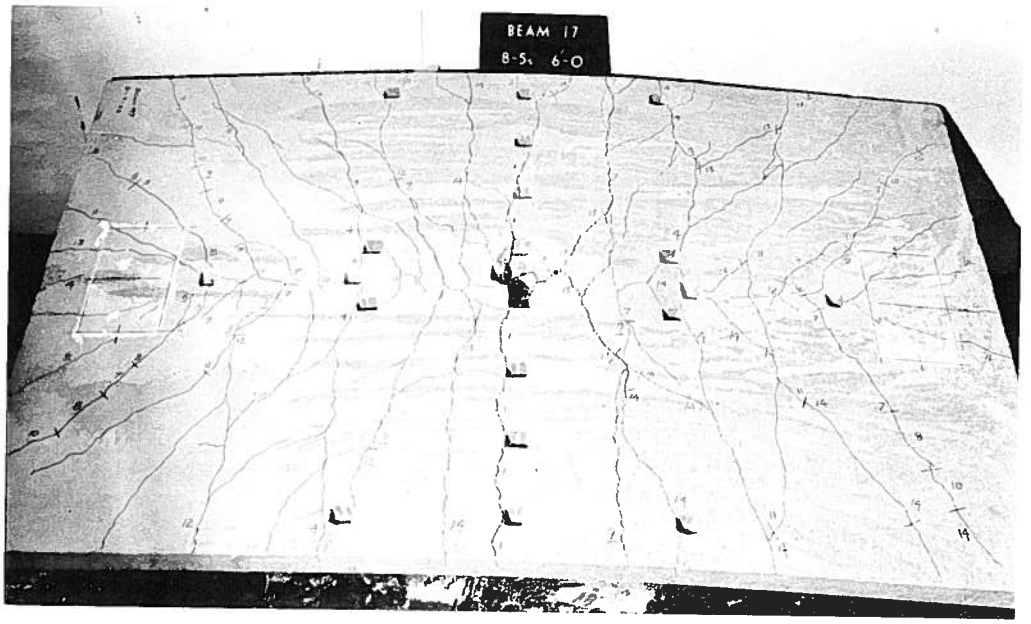

PLATE 3.5 CRACK PATTERNS

CHAPTER IV

DISCUSSION OF TEST RESULTS

4.1 GENERAL BEHAVIOR

It was evident that in each test a complete plastic hinge was developed before the specimen began to unload due to local buckling. The lateral bracing system prevented lateral buckling of the compression flange prior to local buckling of the web and compression flange. A desirable characteristic of the general behavior was the absence of a sudden failure after local buckling. In all tests it was possible to determine several points on the unloading portion of the load-deflection curve.

PLATE 3.1 illustrates the short region over which the flange local buckles occurred. This characteristic is typical of beams under high moment gradient.

Two distinct yield patterns developed in the web near failure as illustrated in PLATE 3.2. In Beams 11, 12, 13, 16 and 17 a horizontal yield line developed at the position of the neutral axis over the entire length of the web. When the yield line developed, the shear was in the order of 80 - 90% of the ultimate shear as determined by CSA Standard S16[9]:

$$V_u = 0.55\ F_y wd$$

Thus, the yielding of the web at the neutral axis was largely due to the high level of shear stress present. Beams 14 and 15 did not exhibit

a horizontal yield line, possibly because of the proximity of the neutral axis to the tension flange. However, vertical shear lines developed throughout the length of the webs of these two beams due to high shear stresses.

4.2 LOAD-DEFLECTION RELATIONSHIPS

The load-deflection relationships presented in FIGURES 3.1 and 3.2 indicate that large plastic deformations occurred before ultimate load was reached. It is also evident that in all tests unloading after local buckling was gradual.

FIGURE 3.1, plotted for all beams having 4'-0" slab width, shows that for any given load, deflection decreased with increase in amount of longitudinal reinforcement. The more heavily reinforced beams attained greater ultimate loads than those less heavily reinforced.

FIGURE 3.2 indicates the effect of varying slab width on the load-deflection relationship. Beams 13, 16 and 17, each containing 8 #5 longitudinal bars, all reached approximately the same ultimate load. Beams 14 and 15, containing 12 #5 longitudinal bars, reached approximately the same ultimate load. No basic difference in the load-deflection relationship existed within either group, indicating that slab width has little effect on deflection.

4.3 MOMENT-CURVATURE RELATIONSHIPS

Curvatures plotted in FIGURES 3.3, 3.4, 3.5 and 3.6 were derived from strain distributions across the WF section. At large strains some of the gages ceased to function and accordingly the

computed curvatures were based on fewer gages located closer to the neutral axis. After buckling of the web it became impossible to determine curvatures with any reasonable degree of accuracy. Thus, the unloading portions of the moment-curvature plots are not shown.

Bending moment is plotted against curvature for Beams 11, 12, 13, 14 and 18 in FIGURE 3.3. As expected, the curvature of a more heavily reinforced beam was less than the curvature of a less heavily reinforced section at any given moment. The ultimate moment capacity varied directly with the amount of longitudinal slab reinforcement. All beams exhibited extensive plastic deformations before their ultimate moment values were reached.

The slope of the moment-curvature relationships in the plastic region was very similar for Beams 11, 12, 13 and 18. The steeper slope of the moment-curvature relationship for Beam 14 is probably due to the proximity of the neutral axis to the tension flange which resulted in a relatively large increase in compression flange strain for a given increment in curvature. Since the moment capacity of the section is highly dependent on the strain in the compression flange, the curvature required to produce a given increase in moment capacity is less for a section with its neutral axis near the tension flange.

Moment-curvature relationships for beams with identical longitudinal reinforcement and varying slab widths are shown in FIGURE 3.4. No significant difference is noted in the ultimate moment capacity or behavior of the beams within either of the two groups.

FIGURES 3.5 and 3.6 relate the M/M_p ratio to curvature. Beams with different areas of longitudinal reinforcement exhibit essentially

the same moment-curvature relationship when the moment value is non-dimensionalized as the ratio of M/M_p. However, the amount of longitudinal reinforcement does effect the curvature at which buckling of the web and compression flange occurs, as evidenced in the variation of ultimate curvature for the test beams.

As indicated in FIGURE 3.6, slab width has little effect on the non-dimensionalized moment-curvature relationships.

Equilibrium relationships for composite beams in negative bending are developed in Appendix B. A computer program developed by Piepgrass[1] which uses equilibrium principles and an iterative technique to produce moment-curvature relationships is described briefly.

4.4 ROTATION CAPACITY

All the beams in the present investigation developed plastic hinges before local buckling of the web and compression flange occurred. However, the curvature at which unloading of the section began varied inversely with the amount of longitudinal slab reinforcement present. Increasing the amount of reinforcement moves the neutral axis of the composite section toward the tension flange. Thus, for any given curvature, a greater portion of the web will be in compression and the maximum compressive strain will be higher. The average strain in the compression flange will also be higher. In this way the amount of longitudinal slab reinforcement affects the stability conditions, particularly of the web, and limits the rotation capacity of the negative plastic hinge.

4.5 LONGITUDINAL REINFORCEMENT STRAINS AT MIDSPAN

Strains in the longitudinal reinforcement across the width of the slab at midspan are described in FIGURES 3.7, 3.8 and 3.9. Generally these strains were uniform at low loads. As the loads increased, strains increased more rapidly in bars near the longitudinal centreline of the beam than in bars near the slab edges. All longitudinal bars reached yield strain well before ultimate load was reached.

Comparison of longitudinal reinforcement strains in Beams 13, 16 and 17, and in Beams 14 and 15 indicates that at any given load the average strain in the wider slabs was as great as that in the narrower slabs. Strain gradients across the wide slabs were no greater than for the narrow slabs. These similarities were expected as a result of the similarities in load-deflection and moment-curvature relationships for beams of varying slab width.

4.6 TRANSVERSE BENDING OF THE CONCRETE SLAB

As indicated in FIGURE 3.10 the centreline and edges of the slab deflected at approximately the same rate until the moment exceeded the simple plastic value. However, as the load approached its ultimate value, the centreline of the beam began to deflect at a much faster rate than the edges of the slab. The relative deflections for Beams 11 and 12 at ultimate load were greater than those for the other beams, probably because Beams 11 and 12 contained less transverse slab reinforcement.

As expected, strains in the transverse slab reinforcement at midspan followed much the same pattern as the relative deflections, as seen in FIGURE 3.11. The strains in the transverse reinforcement

reached the yield value at ultimate load, even though the area of transverse reinforcement was 2.29 or 3.02 times temperature and shrinkage requirements.

4.7 CRACKING OF THE CONCRETE SLAB

PLATES 3.3 and 3.4 illustrate the crack patterns in the slabs of the test beams. The major transverse cracks coincided with locations of transverse reinforcing bars. Generally, cracks near midspan were perpendicular to the longitudinal axis of the beam, but at locations closer to the supports, the cracks tended to curve towards the end of the beam as they approached the slab edges. Diagonal cracks formed near failure, probably due to a combination of high shear transfer and transverse bending of the slab.

4.8 ULTIMATE LOAD CONDITIONS

Ultimate moment capacities for the test beams are given in TABLE 3.1. In FIGURE 3.12 the ratio of M_{ult}/M_p is plotted as a function of $A_s f_y$, the total tensile force in the longitudinal slab reinforcement at yield. The M_{ult}/M_p ratio decreased linearly with increase in the amount of longitudinal reinforcement. As the amount of reinforcement was increased the web of the WF section became more susceptible to buckling and the M_{ult}/M_p value was thereby reduced. However, due to the low width-thickness ratios for the flange and web of the 12WF36 section, the lowest M_{ult}/M_p value was 1.20, even though the neutral axis for the fully yielded condition was in the tension flange. The ratio of M_{ult}/M_p for the WF section alone was 1.42. Thus the lower bound value of the ratio of M_{ult}/M_p was 85%

of that for the WF alone.

FIGURE 3.13 shows the increase in moment capacity due to the addition of longitudinal slab reinforcement. Values of the ratio M_{ult}/M^{o}_{ult} are plotted as a function of $A_s f_y$. A plot of M_p/M^{o}_{p} versus $A_s f_y$ is shown for comparison. The increase in ultimate moment capacity with increased slab reinforcement is not as great as the increase in plastic moment capacity would predict. The difference between the experimental ultimate and theoretical simple plastic moment values is greater in the more heavily reinforced beams. This difference is attributable to the assumption that the plastic moment capacity is achieved prior to local buckling. This assumption does not necessarily hold for the case of a composite beam because of the difference in the stability conditions of the web.

FIGURE 3.14 shows the rotation capacity at ultimate moment for the beams tested. From the plot it is seen that the ratio of ultimate moment to the simple plastic moment capacity of the composite section increases as the ratio of ϕ_{ult}/ϕ'_{p} increases. Due to the stocky nature of the WF section used, all beams exhibited large rotation capacities. Values of ϕ_{ult}/ϕ'_{p} (the ratio of curvature at ultimate moment to curvature at the theoretical plastic moment capacity of the composite member) ranged from 9.1 for the most heavily reinforced beam to 32.9 for the most lightly reinforced beam. The value of ϕ_{ult}/ϕ'_{p} for the WF was 36.5.

Also shown on the figure are values obtained in the negative bending tests of Piepgrass[1] and the positive bending test of Ferrier[8]. Piepgrass' test beams employed a 12B16.5 as the standard steel section,

with coverplates added to the compression flange to prevent premature local buckling. A 12B16.5, although classified as compact by CSA Standard S16 for G40.12 steel, has width-thickness ratios near the limits for a compact section. The values of ϕ_{ult}/ϕ_p' obtained in Piepgrass' tests (1.9 to 4.3) indicate that even if a composite beam contains a compact section it may have very low rotation capacity. A composite beam with such a light steel section would not undergo a complete redistribution of moments to the positive moment section of the beam, and therefore would be considered unsuitable for plastic design.

Values of ϕ_{ult}/ϕ_p' for Ferrier's positive moment tests ranged from 4.5 to 11.4. The actual values of curvature at the computed failure moment ranged from 0.000228 to 0.000430. Thus all beams tested in the present investigation possessed adequate rotation capacity to fully develop the plastic moment capacity of a positive moment section as defined in Ferrier's tests.

CHAPTER V

SUMMARY, CONCLUSIONS AND RECOMMENDATIONS

5.1 SUMMARY

The objective of this investigation was to determine the effect of longitudinal slab reinforcement on the moment and rotation capacities of composite beams in an isolated negative moment region. Eight tests were performed on beams with varying slab widths and amounts of reinforcement. A relatively stocky WF section was employed to minimize the possibility of premature failure due to local buckling. All beams exhibited large rotations after yielding occurred at the location of the negative plastic hinge. Failure was initiated by local buckling in the web. Unloading was gradual after the subsequent development of a local buckle in the compression flange.

5.2 CONCLUSIONS

The following conclusions can only be directly applied to composite beams with a 12WF36 as the steel section. Lighter steel sections may not exhibit adequate rotation capacity required to develop the simple plastic moment for the composite section in negative bending. In a continuous member, a relatively light section, although able to develop the negative simple plastic moment, may not possess the necessary rotation capacity required to sustain this moment until the full moment capacity of the beam develops at positive bending locations.

It is noted from the work of Piepgrass[1] that a steel section classified as compact by CSA Standard S16 does not necessarily possess such rotation capacity when used in a composite beam.

The following conclusions can be made on the basis of the present investigation:

1. Significant increases in the negative moment capacity of composite beams can be achieved by the addition of longitudinal slab reinforcement, but these increases are not in proportion to theoretical simple plastic moment values. The exact contribution of the longitudinal steel cannot be established from the present investigation but it is related to the effect of the reinforcement on the stability conditions of the web. The lower bound value of M_{ult}/M_p for the test series was 1.20, compared to a value of 1.42 for the WF section alone.

2. As the amount of longitudinal slab reinforcement is increased, the rotation capacity of the negative plastic hinge decreases. Thus if a particular rotation capacity is required at a negative hinge location in a continuous composite beam in order to develop a subsequent positive moment hinge and thereby produce a mechanism, there is a limit on the amount of longitudinal reinforcement that can be employed.

3. For a given amount of longitudinal reinforcement, variation in slab width, within the limits permitted by CSA Standard S16, has no significant effect on ultimate moment capacity or rotation capacity.

4. Provided buckling of the steel section can be prevented, all the longitudinal slab reinforcement reaches the yield condition prior to ultimate moment. However, the corresponding curvature is greater than predicted from a linear strain distribution across the steel section.

5. The test beams possessed sufficient rotation capacity for complete redistribution of moments and the formation of a mechanism in a continuous beam for cases where negative hinges are first to form.

5.3 RECOMMENDATIONS

On the basis of this investigation, it is recommended that the full contribution of the longitudinal slab reinforcement not be employed in calculation of the simple plastic moment capacity of composite beams in negative bending.

It is also recommended that effective slab widths as specified by CSA Standard S16 for positive bending be adopted for negative bending also.

LIST OF REFERENCES

1. Piepgrass, E.B., "Behavior of Composite Beams in Negative Bending", Masters Thesis, Department of Civil Engineering, University of Alberta, June 1968.

2. Siess, C.P., and Viest, I.M., "Test of Continuous Right I-Beam Bridges", University of Illinois Engineering Experiment Station, Bulletin Series No. 416.

3. Culver, C., Zarzeczny, P.J., and Driscoll, G.C. Jr., "Test of Composite Beams for Buildings", Progress Report 2, Fritz Engineering Laboratory Report No. 279.6, January, 1961.

4. Slutter, R.G.., and Driscoll, G.C. Jr., "Test Results and Design Recommendations Composite Beams for Buildings", Progress Report 3, Fritz Engineering Laboratory Report No. 279.10, January 1962.

5. Barnard, Peter R., "On the Collapse of Composite Beams", a dissertation submitted to the University of Cambridge for the degree of Doctor of Philosophy, Corpus Christi College, September 1963.

6. Daniels, J.H., and Fisher, J.W., "Fatigue Behavior of Continuous Composite Beams", Fritz Engineering Laboratory Report No. 324.1, December 1967.

7. Daniels, J.H., and Fisher, J.W., "Static Behavior of Continuous Composite Beams", Fritz Engineering Laboratory Report No. 324.2, March 1967.

8. Ferrier, D., "Moment Curvature Relationship of Composite Steel and Concrete Beams", Masters Thesis, Department of Civil Engineering, University of Alberta, November 1965.

9. Canadian Standards Association Standard S16-1965, "Steel Structures for Buildings", December 1965.

NOMENCLATURE

A_c	area of concrete in slab
A_s	area of longitudinal slab reinforcement
A_t	area of transverse slab reinforcement
A_{WF}	area of wide flange section
b	width of flange
d	depth of steel section
F_y	yield stress of WF section
f_y	yield stress of longitudinal slab reinforcement
h	clear depth of web
M	moment
M_p	theoretical simple plastic moment
M_p^o	theoretical simple plastic moment for 12WF36
M_{ult}	ultimate moment
M_{ult}^o	ultimate moment for 12WF36
P_{ult}	ultimate load
r_y	radius of gyration about vertical axis
t	thickness of flange
V_u	ultimate shear force
w	thickness of web
ϕ_{ult}	curvature at ultimate moment
ϕ_p'	theoretical curvature at simple plastic moment

ACKNOWLEDGEMENTS

This investigation is part of a continuing project "Behavior of Composite Flexural Members" in progress in the Department of Civil Engineering, University of Alberta. This project is sponsored financially by the National Research Council of Canada.

The assistance of Mr. H. Panse and members of the laboratory staff in the fabrication and testing of the beam specimens, and Mrs. K. Davison, who typed the manuscript, is acknowledged.

APPENDIX A

MATERIAL PROPERTIES

TABLE A.1

CONCRETE DATA

BEAM	AGE AT TEST (days)	COMPRESSIVE STRESS (psi)	SPLITTING TENSION (psi)
11	7	4350	583
	54	5230	673
	54	5310	679
12	7	4600	555
	62	4540	521
	62	5050	555
13	10	4780	693
	39	5160	502
	39	5680	389
14	7	3500	610
	67	4370	539
	67	4130	582
15	7	4270	392
	64	5120	486
	64	5000	633
16	10	4620	556
	41	4420	607
	41	4840	556
17	7	4080	368
	71	5030	439
	71	5070	484

MIX PROPORTIONS

Cement (high early)	133 lbs.
Sand	344 lbs.
Coarse Aggregate	500 lbs.
Water	66 lbs.(approximately)

Slump 3½"

TABLE A.2

SLAB REINFORCEMENT DATA

TYPE	YIELD STRESS (ksi)	ULTIMATE STRESS (ksi)
#3 BAR	53.2 52.7 52.2 52.7 52.7 52.7	75.0 75.0 75.0 75.0 75.5 76.3
	Ave. 52.7	75.4
#4 BAR	55.0 54.8 55.2 55.0 55.8 56.0	83.3 83.5 84.2 83.8 84.8 83.8
	Ave. 55.3	83.9
#5 BAR	52.6 52.9 52.2 52.4 53.2 53.6	80.9 81.8 81.5 82.0 81.8 82.1
	Ave. 52.8	81.7

TABLE A.3

STEEL BEAM PROPERTIES

TYPE	YIELD STRESS (ksi)	ULTIMATE STRESS (ksi)	MODULUS OF ELASTICITY (ksi)	STRAIN AT STRAIN HARDENING (in/in)	STRAIN HARDENING MODULUS (ksi)
FLANGE	40.4	67.7	29700	0.0057	857
	39.8	67.7		0.0081	658
	39.2	67.9	28800	0.0066	725
	39.7	67.8	27600	0.0106	738
	Ave. 39.8	67.8	28700	0.0078	745
WEB	46.4	69.2	27600	0.0144	
	43.5	69.2	29400	0.0170	593
	Ave. 45.0	69.2	28500	0.0157	593

APPENDIX B

THEORETICAL MOMENT-CURVATURE RELATIONSHIPS

The equilibrium relationships for composite beams in negative bending are given for three strain conditions encountered during the loading of such a beam to failure. Case 1 is the elastic case. In Case 2 the compression flange and a portion of the web have reached yield. In Case 3 the longitudinal slab reinforcement and the tension flange have yielded and the compression flange is in the strain hardening range. The theoretical fully plastic case is considered as Case 4. In all cases the force in a flange is considered to act through the flange centroid. The resulting error in the moment contribution is not significant.

NOTATION

b	width of flange
C^f	compressive force in flange
C^w	compressive force in web
C^f_y	compressive force in flange at yield
C^w_y	compressive force in web at yield
C^f_{st}	additional compressive force in flange due to strain hardening
C^w_{st}	additional compressive force in web due to strain hardening
d	depth of steel section
d_s	distance from tension flange to centroid of longitudinal reinforcement
E	modulus of elasticity of steel
E_{st}	strain hardening modulus of steel

e	strain
e^f	maximum tension flange strain
e^s	strain in longitudinal reinforcement
e^w	strain in web
e_o	maximum compression flange strain
e^s_{proj}	strain at the level of the longitudinal reinforcement obtained as a projection of the strain distribution across the WF section
e_y	yield strain
e^f_y	strain in flange at yield
e^s_y	strain in longitudinal reinforcement at yield
e^w_y	strain in web at yield
e_{st}	strain at strain hardening
e^f_{st}	strain in flange at strain hardening
e^w_{st}	strain in web at strain hardening
i	interaction factor
M	moment
M_{ext}	applied moment
M_p	simple plastic moment
N.A.	neutral axis
T^f	tensile force in flange
T^s	tensile force in longitudinal reinforcement
T^w	tensile force in web
T^f_y	tensile force in flange at yield
T^s_y	tensile force in longitudinal reinforcement at yield
T^w_y	tensile force in web at yield
t	thickness of flange

w	thickness of web
y_c	distance from neutral axis to outside of compression flange
ϕ	curvature
σ	stress
σ_y	yield stress
ΣF	sum of horizontal forces
ΣM	sum of moments about the neutral axis
A_s	area of longitudinal slab reinforcement

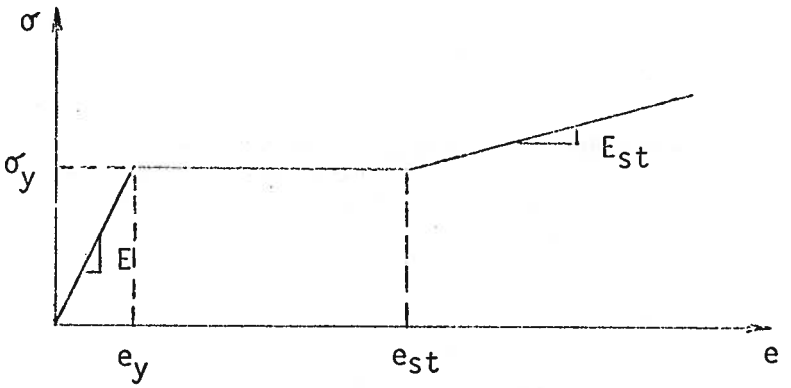

IDEALIZED STRESS-STRAIN RELATIONSHIP FOR STEEL

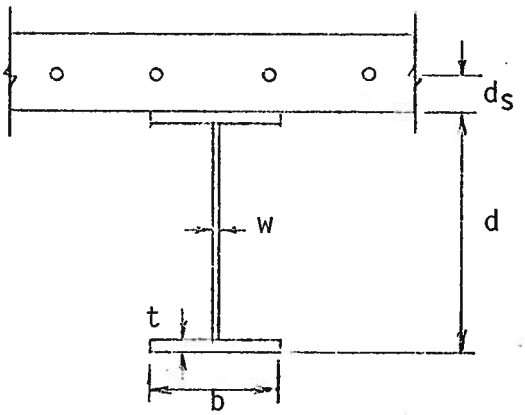

DIMENSIONS OF COMPOSITE SECTION

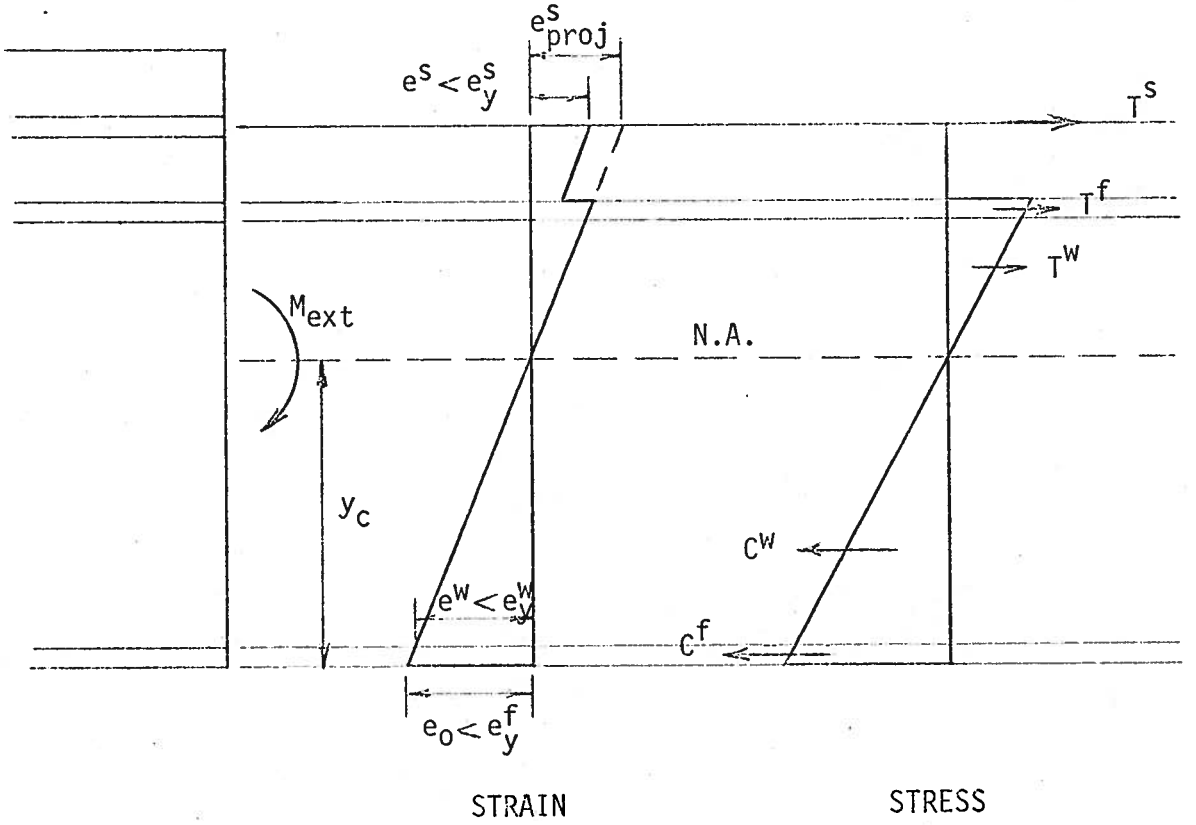

CASE 1 ELASTIC CONDITIONS

$$\text{INTERACTION FACTOR } i = \frac{e^s}{e^s_{proj}}$$

$\Sigma F=0$:

$$E\frac{e_o}{y_c}\left[A_s\, i\,(d+d_s-y_c) + b\,t\,(d-y_c-\tfrac{1}{2}t) + \frac{1}{2}w\,(d-y_c-t)^2 - \frac{1}{2}w\,(y_c-t)^2 - b\,t\,(y_c-\tfrac{1}{2}t)\right] = 0 \qquad (1)$$

$\Sigma M=0$:

$$E\frac{e_o}{y_c}\left[A_s\, i\,(d+d_s-y_c)^2 + b\,t\,(d-y_c-\tfrac{1}{2}t)^2 + \frac{1}{3}w\,(d-y_c-t)^3 + \frac{1}{3}w\,(y_c-t)^3 + b\,t\,(y_c-\tfrac{1}{2}t)^2\right] = M_{ext} \qquad (2)$$

FOR SMALL ANGLES $\phi = \frac{e_o}{y_c}$ (3)

The value of y_c is determined from equation (1) from the properties of the section and the material properties. The relationship between M_{ext} and ϕ may then be determined from equations (2) and (3).

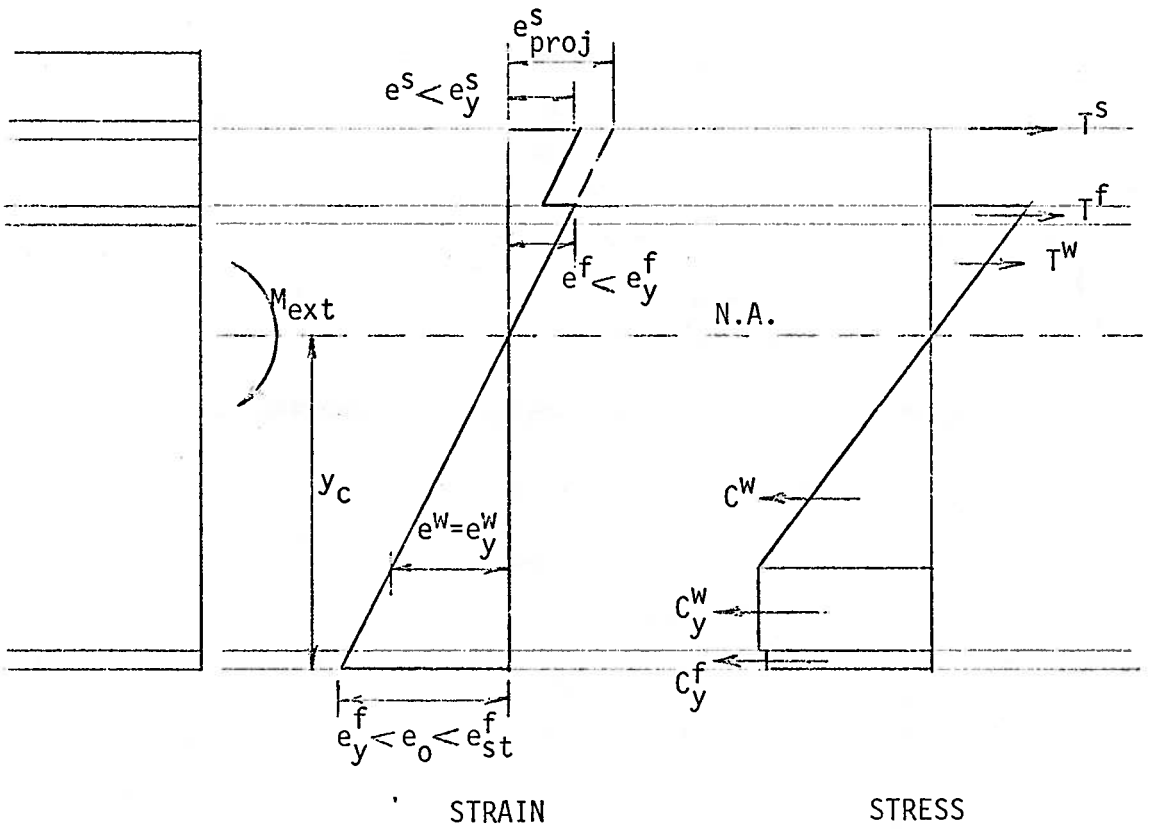

CASE 2 YIELDING IN THE COMPRESSION ZONE

$\Sigma F=0$:

$$E\left[A_s\, i\, \frac{e_o}{y_c}(d+d_s-y_c) + b\, t\, \frac{e_o}{y_c}(d-y_c-\tfrac{1}{2}t) + \frac{1}{2}\, w\, \frac{e_o}{y_c}(d-y_c-t)^2 - w\, e^w_y\,(y_c-t-\tfrac{1}{2}\,\frac{e^w_y}{e_o}\,y_c) - b\, t\, e^f_y\right] = 0 \qquad (1)$$

$\Sigma M=0$:

$$E\left[A_s\, i\, \frac{e_o}{y_c}(d+d_s-y_c)^2 + b\, t\, \frac{e_o}{y_c}(d-y_c-\tfrac{1}{2}t)^2 + \frac{1}{3}w\,\frac{e_o}{y_c}(d-y_c-t)^3 + \frac{1}{3}w\,(\frac{e_y^w}{e_o}y_c)^2\, e_y^w + \frac{1}{2}w\,(y_c-t-\frac{e_y^w}{e_o}y_c)\, e_y^w\,(y_c-t+\frac{e_y^w}{e_o}y_c) + b\, t\, e_y^f\,(y_c-\tfrac{1}{2}t)\right] = M_{ext} \qquad (2)$$

$$\phi = \frac{e_o}{y_c} \qquad (3)$$

Substitution of $e_o = \phi\, y_c$ from equation (3) into equations (1) and (2) results in two equations with three unknowns - y_c, M_{ext} and ϕ. For any given value of ϕ these equations may be solved simultaneously for the corresponding values of y_c and M_{ext}.

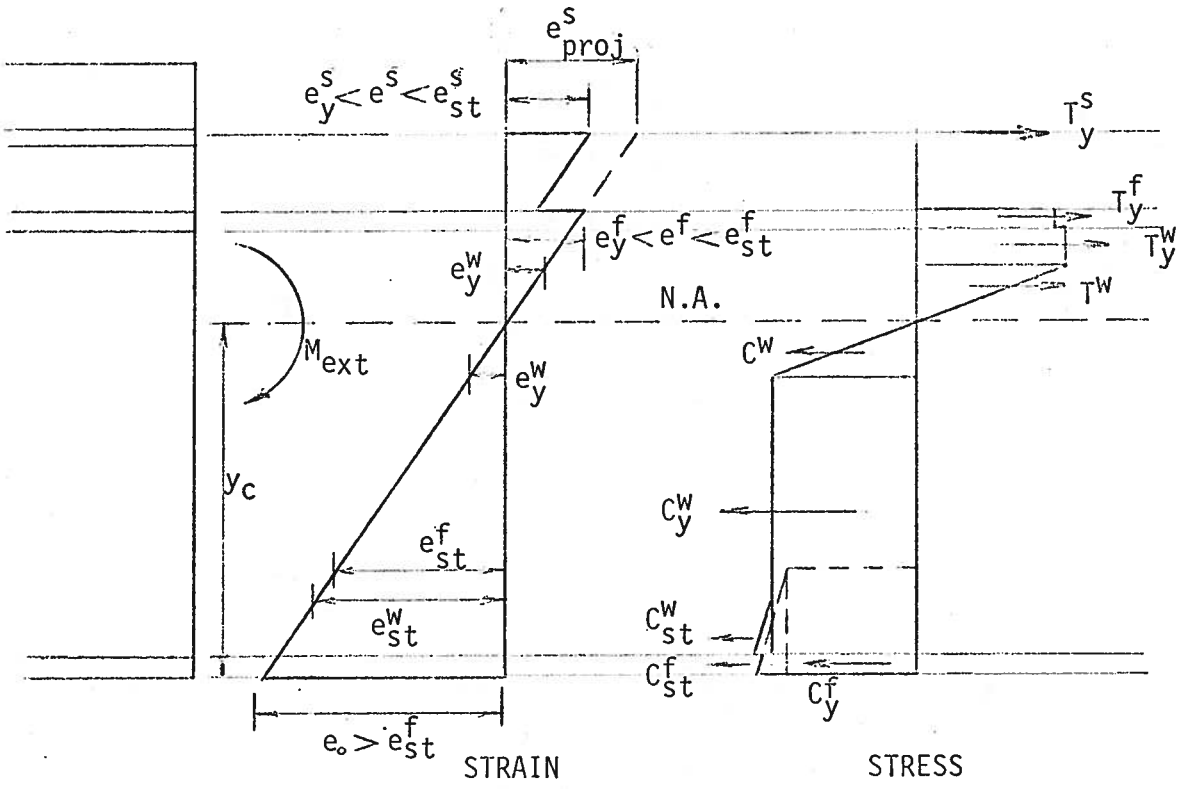

CASE 3 STRAIN HARDENING IN COMPRESSION ZONE

$\Sigma F=0$:

$$A_s\ E\ e_y^s + b\ t\ E\ e_y^f + w\ (d-2y_c)\ E\ e_y^w - \frac{1}{2}\ w \frac{(y_c - t - \frac{e_{st}^w}{e_o}\ y_c)^2}{(y_c - \frac{e_{st}^w}{e_o}\ y_c)}\ E_{st}\ e_o$$

$$- b\ t \left[E\ e_y^f + E_{st}\ e_o \frac{(y_c - t - \frac{e_{st}^f}{e_o}\ y_c)}{(y_c - \tfrac{1}{2}t - \frac{e_{st}^f}{e_o}\ y_c)} \right] = 0 \qquad (1)$$

$\Sigma M=0$:

$$A_s\ E\ e_y^s\ (d+d_s-y_c) + b\ t\ E\ e_y^f\ (d-y_c-\tfrac{1}{2}t)$$

$$+ \frac{1}{2}\ w\ (d-y_c-t-\frac{e_y^w}{e_o}\ y_c)\ E\ e_y^w\ (d-y_c-t+\frac{e_y^w}{e_o}\ y_c)$$

$$+ \frac{2}{3}\ w\ (\frac{e_y^w}{e_o}\ y_c)^2\ e_y^w$$

$$+ \frac{1}{2}\ w\ (y_c-t-\frac{e_y^w}{e_o}\ y_c)\ E\ e_y^w\ (y_c-t+\frac{e_y^w}{e_o}\ y_c)$$

$$+ \frac{1}{3}\ w\ (y_c-t-\frac{e_{st}^w}{e_o}\ y_c)^2\ E_{st}\ e_o \frac{(\frac{1}{2}\frac{e_{st}^w}{e_o}\ y_c+y_c-t)}{(y_c-\frac{e_{st}^w}{e_o}\ y_c)}$$

$$+ \left[b\ t\ E\ e_y^f + b\ t\ E_{st}\ e_o \frac{(y_c-t-\frac{e_{st}^f}{e_o}\ y_c)}{(y_c-\frac{1}{2}t-\frac{e_{st}^f}{e_o}\ y_c)} \right] (y_c-\tfrac{1}{2}t) = M_{ext} \qquad (2)$$

$$\phi = \frac{e_o}{y_c} \qquad (3)$$

The equations may be solved in the same manner as for Case 2.

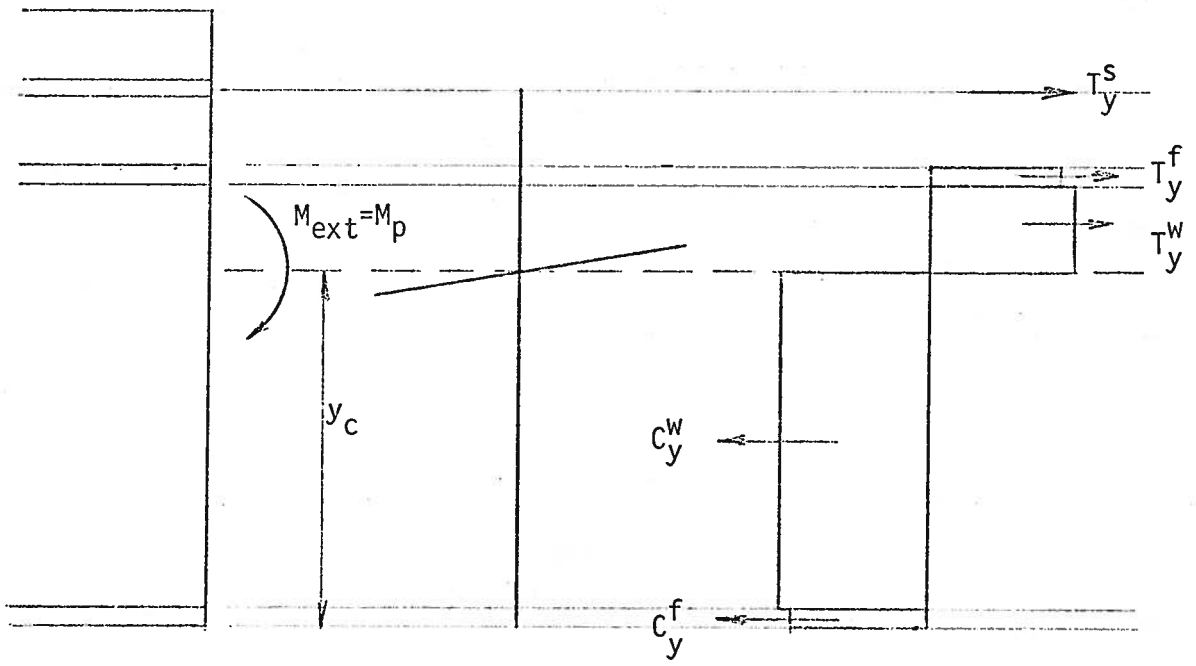

CASE 4 FULLY PLASTIC SECTION - NO STRAIN HARDENING

$\Sigma F=0$:

$$E\left[A_s\, e_y^s + b\, t\, e_y^f + w\,(d-y_c-t)\, e_y^w - w\,(y_c-t)\, e_y^w - b\, t\, e_y^f\right] = 0$$

from which $$y_c = \frac{d}{2} + \frac{A_s\, e_y^s}{2w\, e_y^w} \qquad (1)$$

$\Sigma M=0$:

$$E\left[A_s\, e_y^s\,(d+d_s-y_c) + b\, t\, e_y^f\,(d-t) + \frac{1}{2}\, w\, e_y^w \left((d-y_c-t)^2 + (y_c-t)^2\right)\right]$$

$$= M_p \qquad (2)$$

Equation (1) defines y_c for the particular dimensions and material properties of the composite section. Substituting this value for y_c in equation (2) gives the simple plastic moment capacity for the section. To achieve the strain distribution assumed would require infinite curvature with no strain hardening.

A computer program was developed by Piepgrass[1] to produce theoretical moment-curvature relationships for composite beams in negative bending. For a given curvature the position of the neutral axis is assumed and the resulting stress distribution is determined from the stress-strain relationships for the longitudinal reinforcement, flange and web steel. The position of the neutral axis is adjusted until the resultant forces in the cross-section are in equilibrium. Having established the position of the neutral axis it is then possible to determine the external moment on the section corresponding to the given curvature. By incrementing the curvature a complete moment-curvature relationship can be determined for any interaction factor. The program has no means of predicting instability of the steel section, and therefore moment rises indefinitely with increased curvature. A typical theoretical moment-curvature relationship with an interaction factor of 1.0 is shown in FIGURE B.1 for Beam 12 of the present investigation. The average material properties presented in Appendix A were used in the computations.

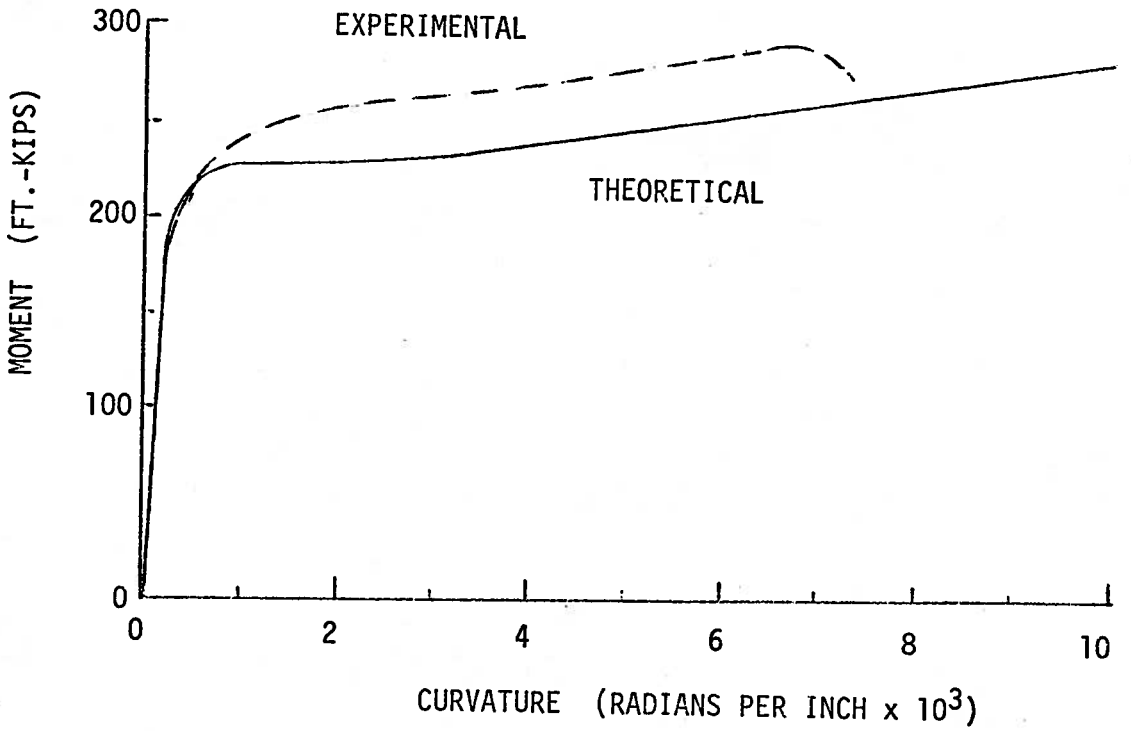

FIGURE B.1 MOMENT-CURVATURE RELATIONSHIP FOR BEAM 12